# The sources of jet noise: experimental evidence

## CHRISTOPHER K. W. TAM[1], K. VISWANATHAN[2], K. K. AHUJA[3] AND J. PANDA[4]

[1]Florida State University, Tallahassee, FL 32306-4510, USA
[2]The Boeing Company, Seattle, WA 98124, USA
[3]Georgia Institute of Technology, Atlanta, GA 30332-0844, USA
[4]NASA Ames Research Center, Moffett Field, CA 94035, USA
tam@math.fsu.edu

The primary objective of this investigation is to determine experimentally the sources of jet mixing noise. In the present study, four different approaches are used. It is reasonable to assume that the characteristics of the noise sources are imprinted on their radiation fields. Under this assumption, it becomes possible to analyse the characteristics of the far-field sound and then infer back to the characteristics of the sources. The first approach is to make use of the spectral and directional information measured by a single microphone in the far field. A detailed analysis of a large collection of far-field noise data has been carried out. The purpose is to identify special characteristics that can be linked directly to those of the sources. The second approach is to measure the coherence of the sound field using two microphones. The autocorrelations and cross-correlations of these measurements offer not only valuable information on the spatial structure of the noise field in the radial and polar angle directions, but also on the sources inside the jet. The third approach involves measuring the correlation between turbulence fluctuations inside a jet and the radiated noise in the far field. This is the most direct and unambiguous way of identifying the sources of jet noise. In the fourth approach, a mirror microphone is used to measure the noise source distribution along the lengths of high-speed jets. Features and trends observed in noise source strength distributions are expected to shed light on the source mechanisms. It will be shown that all four types of data indicate clearly the existence of two distinct noise sources in jets. One source of noise is the fine-scale turbulence and the other source is the large turbulence structures of the jet flow. Some of the salient features of the sound field associated with the two noise sources are reported in this paper.

## 1. Introduction

For more than half a century, Lighthill's acoustic analogy (1952, 1954) has been, unquestionably, the dominant jet noise theory. Within the framework of acoustic analogy, the sources of jet mixing noise are quadrupoles. Over the years, Lighthill's acoustic analogy has spawned many variants of the basic theory; e.g. Proudman (1952), Lilley (1958), Doak (1960), Phillips (1960), Ffowcs Williams (1963), Ribner (1964), and Goldstein & Rosenbaum (1973), to name just a few. The source terms of the various modified acoustic analogy theories are not the same; but in the literature, their sources of noise have all been loosely referred to as quadrupoles. Among the variants of the original theory, Lilley's approach appears to have attracted the largest
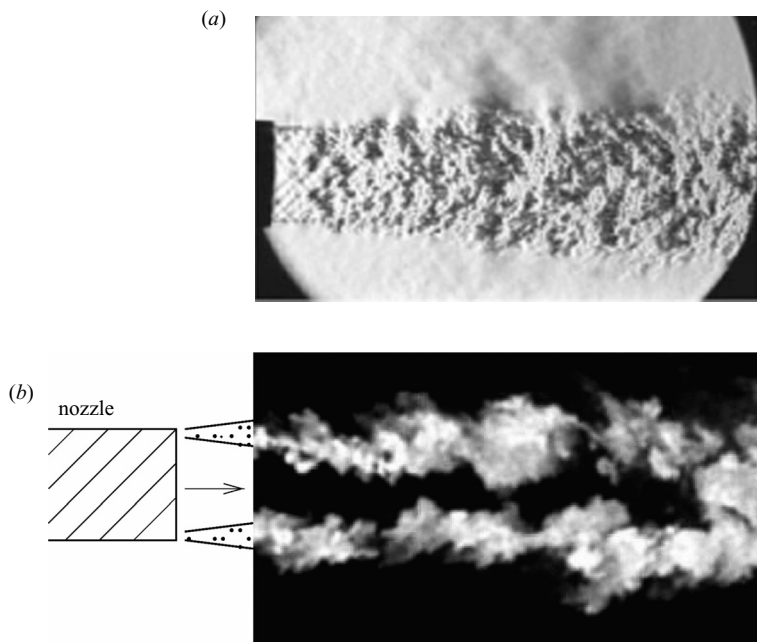
(a)



(b) nozzle

FIGURE 1. (a) Spark schlieren photograph of a Mach 1.4 jet. (b) Pulsed laser picture of the large turbulence structures in the mixing layer of a Mach 1.3 jet (Thurow *et al.* 2003). Reused with permission from Brian Thurow, Physics of Fluids, 15, 1755 (2003). Copyright 2003, American Institute of Physics.

number of followers (e.g. Tester & Morfey 1976; Khavaran *et al.* 1994; Morris & Farassat 2002; Goldstein 2003; Hunter & Thomas 2003; and others).

Schlinker (1975) and Laufer, Schlinker & Kaplan (1976) appear to be the first to propose an alternative jet noise source model. Their model consists of two sources. Their proposed model is based on their own experimental observations. Laufer *et al.* developed a spherical reflector directional microphone to measure the location of jet noise sources. Their reflector or mirror microphone was capable of focusing on a localized region of a jet and measured the noise radiated from this region. They observed that for high supersonic jets, the locations and distributions of the noise sources radiated to the 90° and those radiated to the 150° directions were distinctly different (inlet angle will be used throughout this paper). Also, their omni-directional microphone real-time pressure signal at 90° and 150° had very different characteristics. The real-time signal in the 90° direction was found to be very similar to that of a subsonic jet, random but smooth; however, in the 150° direction, the real-time pressure signature contained numerous shock-like spikes. Laufer *et al.* reasoned that the noise source distributions as well as real-time pressure histories, being so different in the 90° and 150° directions, could only be a direct result of two noise sources.

There is universal agreement that jet mixing noise is generated by the turbulence of the jet flow. Before the 1970s, jet turbulence was thought to consist of numerous small eddies distributed throughout the jet (figure 1a). Figure 1(a) is a spark schlieren photograph of a Mach 1.4 jet. Crow & Champagne (1971) and Brown & Roshko (1974) were the first to report the observation of large coherent structures in turbulent jets and free shear layers. This was in addition to classical small-scale turbulence. Since their work, there has been an abundance of papers in the literature devoted

to the measurement, study, analysis and numerical simulation of these structures. Figure 1(*b*) is a pulsed laser picture of the large turbulence structures in the mixing layer of a Mach 1.3 jet Thurow, Samimy & Lempert (2003). This picture is typical of most optical observations of large turbulence structures in a turbulent jet flow. It is well known that jet flows are inherently unstable. The large turbulence structures may be regarded as a manifestation of nonlinear instabilities (Kelvin–Helmholtz instability waves grow to nonlinear amplitudes). These structures are generated near the nozzle exit. They grow quickly as they are convected or propagated downstream. They are coherent over distances comparable to and often longer than the jet diameter in the axial direction. Thus, as sources of jet noise, the fine-scale turbulence is a compact source, whereas the large turbulence structures of full-scale jet engines are non-compact sources.

Optical observations such as that shown in figure 1(*b*) indicate that the large turbulence structures are the dominant dynamical entities in the mixing layer of a jet in the region starting from the nozzle exit extending to some distance downstream of the end of the potential core. Further downstream of the potential core, the large turbulence structures decay through merging and cascading to smaller and smaller scale turbulence. It is important to recognize that the most turbulent and dynamically most energetic region of a jet lies in the first two potential core lengths of the jet. Within this region, there is a distinct separation of turbulence scales. (Separation of scales in a mixing layer can easily be observed in optical measurements. A good example is the original pictures taken by Brown & Roshko (1974) in their pioneering paper announcing the discovery of large coherent turbulence structures. Some of these pictures are reprinted in Van Dyke (1982)). The principal scales are those of the small turbulent eddies with dimensions much smaller than the jet diameter and the large turbulence structures with dimensions longer than or comparable to the jet diameter. Optical observations do not indicate a single monotonic spectrum of turbulence scales. Because the fluid residence time in this region is short for high-speed jets, the cascade process that causes turbulence energy to transfer from large to small scales has only limited time to act. A smooth monotonic turbulence spectrum exists only in the decaying portion of the jet flow way downstream.

During the early days of jet noise research, data were routinely measured in 1/3-octave bands. With advances in instrumentation, highly accurate narrowband jet noise data, including those from high-temperature jets, became available in the 1990s. After a thorough analysis of an extensive collection of the NASA Langley Research Center, Jet Noise Laboratory data, Tam, Golebiowski & Seiner (1996) found empirically two seemingly universal spectra that were able to fit all the jet noise spectra in the data bank. This is true regardless of jet Mach number and jet temperature. Figure 2 shows the two similarity spectra plotted as functions of $f/f_{peak}$, where $f$ is the frequency and $f_{peak}$ is the frequency at the peak of the spectrum. The $F$-spectrum or the peaky spectrum fits all noise spectra measured in the downstream directions within a cone around the jet axis. The $G$-spectrum or the broad spectrum fits all noise spectra radiated in the upstream and sideline directions. In the transitional directions a superposition of the contributions from the two spectra is required to fit the measured spectra.

It is not difficult to demonstrate how well the similarity spectra fit measured noise data. As an example, let us use data measured by Seiner *et al.* (1992) and Viswanathan (2004) (these are data measured as a part of their published work and are made available to this investigation) at a total jet temperature to ambient temperature ratio of 1.8 to compare with the similarity spectra. Figure 3 shows the far-field noise spectra, normalized to a distance of 100 fully expanded jet diameters, from three
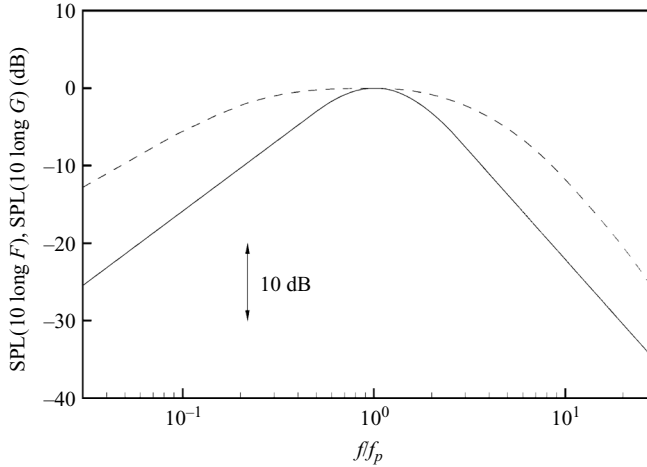
FIGURE 2. Similarity spectra for the two components of turbulent mixing noise:
———, large turbulence structure noise; – – –, fine-scale turbulence noise.

jets at Mach numbers 0.7, 1.5 and 1.96. Figures 3(*a*) to 3(*c*) show how well the
*G*-spectrum fits the data at inlet angles 80°, 90° and 100°. The fitting is done by
placing the peak of the similarity spectrum to coincide with that of the measured
data. Figures 3(*f*) and 3(*g*) show how well the *F*-spectrum fits the measured data
at the 130° and 140° directions. In the transitional directions, at 110° and 120°, a
combination of the two similarity spectra is required in order to produce a spectrum
that fits the measurement. This is shown in figures 3(*d*) and 3(*e*).

   Dahl & Papamoschou (2000) reported that the similarity spectra fitted their mea-
sured coaxial jet noise spectra well. Viswanathan (2002, 2004) provided extensive
comparisons between the similarity spectra and his measurements over a large range of
subsonic Mach numbers and temperature ratios. Tam (1998) compared the similarity
spectra with the extensive jet noise data collection measured by Yamamoto *et al.*
(1984) as well as noise data from non-circular nozzles measured at the NASA
Langley Research Center. Yamamoto *et al.*'s data included jet noise spectra from
*C–D* nozzle, convergent plug nozzle, *C–D* plug nozzle and suppressor nozzle. For
each type of nozzle, two sets of data were compared. One set of data was measured
in a static environment. The other set of data was measured in an open wind tunnel
simulating forward flight. The NASA data were from an elliptic nozzle of aspect ratio
3 and a rectangular nozzle of aspect ratio 7.6 operating at supersonic Mach number.
Tam & Zaman (2000) compared the similarity spectra with subsonic jet noise data
from elliptic, rectangular, tabbed and six-lobe nozzles. Good agreements were found
in all the cases.

   The existence of two seemingly universal similarity spectra offers strong experi-
mental support for the two-noise source model proposed by Tam & Chen (1994)
and Tam (1995). The proposed two-noise sources are quite different from those of
Laufer *et al.* (1976). Figure 4 is a schematic diagram of the two noise sources and
their sound fields. In this model, the two noise sources are the fine-scale turbulence
and the large turbulence structures of the jet flow. Fine-scale turbulence is distributed
throughout the mixing layer of the jet. According to Tam & Auriault (1999), fine-scale
turbulence exerts an effective turbulence pressure on its surroundings. The intensity
of the turbulence pressure is equal to 2/3 of the turbulence kinetic energy. Noise
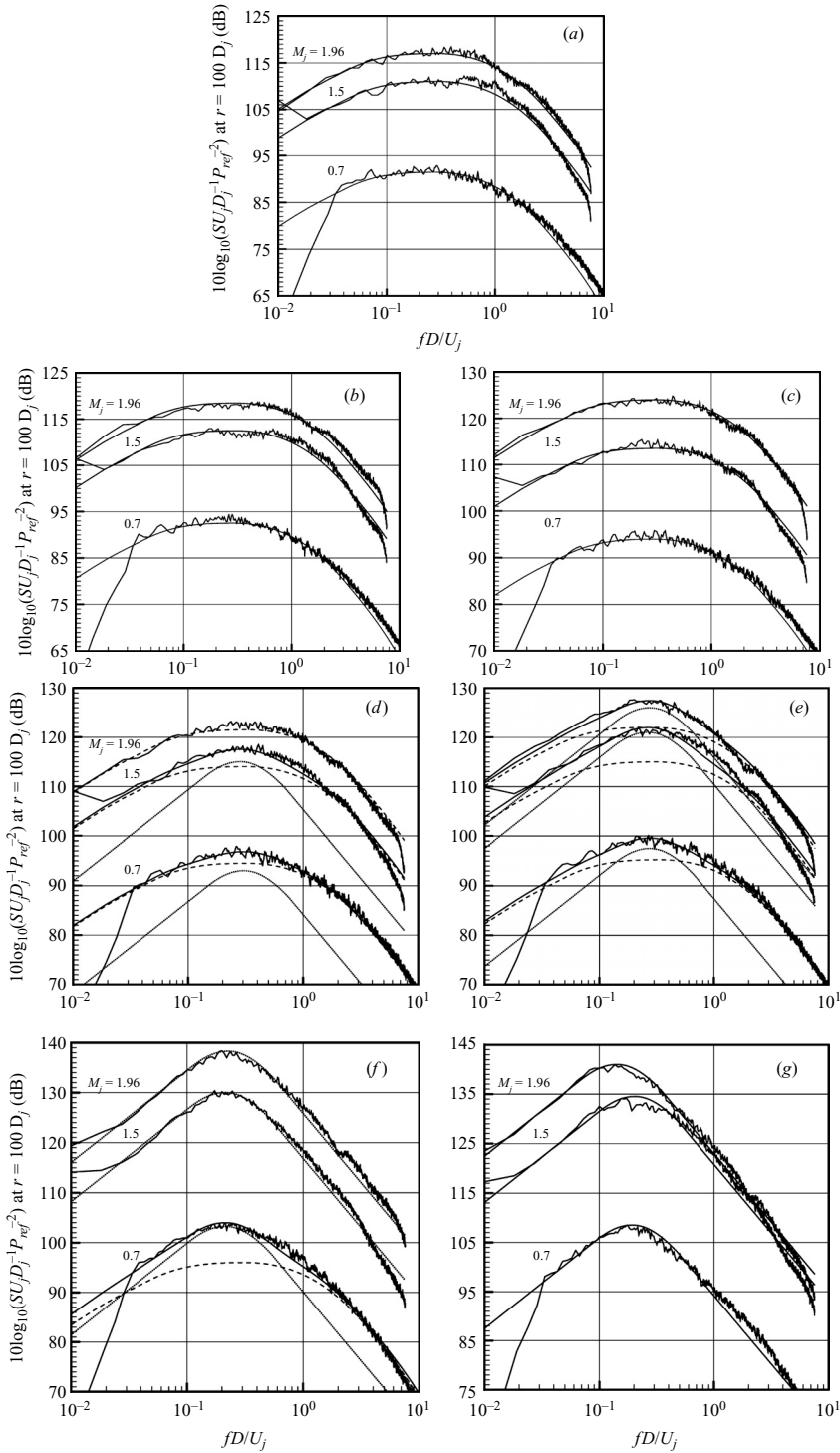is generated when there are fluctuations in the turbulence pressure arising from

FIGURE 3. Comparisons between similarity spectra (smooth curves) and measured spectra by Seiner *et al* (1992) and Viswanathan (2004). $T_r/T_a = 1.8$. (*a*) 80°, (*b*) 90°, (*c*) 100°, (*d*) 110°, (*e*) 120°, (*f*) 130°, (*g*) 140°.
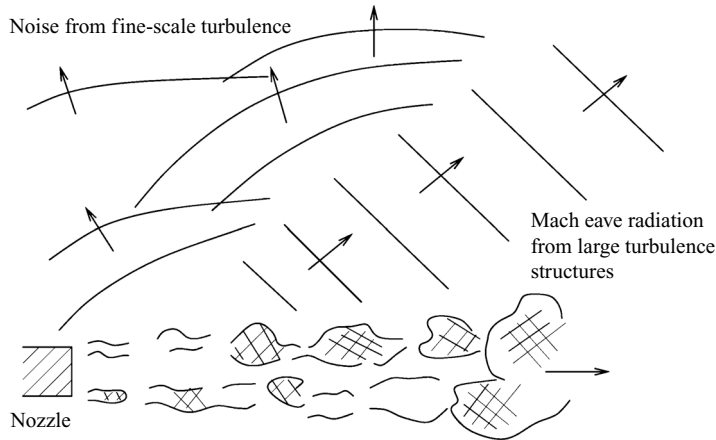
FIGURE 4. Schematic diagram showing the large turbulence structures of a high-speed jet, the sound fields from the fine-scale turbulence and the Mach wave radiation from the large turbulence structures.

fluctuations in turbulence kinetic energy. A blob of fine-scale turbulence is small. The noise radiated is statistically isotropic. However, because the fine-scale turbulence is being transported downstream by the mean flow, this convection effect leads to a slight preference to downstream noise radiation. In addition, the radiated sound from a blob of fine-scale turbulence has to traverse the shear layer of the jet to reach outside. Therefore, the radiated sound will undergo refraction owing to velocity and density gradients in the jet mixing layer. Hence, we would expect the noise from the fine-scale turbulence of the jet to be nearly omni-directional. It is slightly stronger in the downstream direction except in the cone of relative silence (see Atvars, Schubert & Ribner (1965) for an experimental demonstration of the existence of a cone of relative silence). The cone of relative silence is created because of the bending of acoustic waves away from the jet flow direction by refraction. This effect is especially strong for high-speed hot jets.

The large turbulence structures are spatially coherent in the axial direction of the jet. This allows the radiated sound from different parts of the structure to reinforce or cancel each other. This effect results in highly directional noise radiation. For very high-speed jets, a simple way to view the noise-generation mechanism is to regard the large turbulence structures as a wavy wall moving supersonically downstream relative to the ambient gas. This immediately leads to strong highly directional Mach wave radiation (figure 4). It was pointed out by Tam & Chen (1979) that, statistically, large turbulence structures could be mathematically represented by a stochastic instability-wave model. In other words, large turbulence structures and instability waves of a jet have nearly identical characteristics, statistically speaking. Some investigators regard large turbulence structures as instability waves having grown to nonlinear amplitudes. It is well known that instability waves start out at very low amplitude near the nozzle exit. They grow rapidly as they propagate downstream. At some point downstream (the location is frequency dependent) an instability wave reaches its maximum amplitude. Beyond this point, the wave becomes a damped wave. The wave amplitude decreases as the wave propagates further downstream. The same sequence of events appears to be followed by the large turbulence structures, based on optical observations. As was pointed out by Tam & Burton (1984a, b), the growth and decay of the amplitude of the large turbulence structures/instability
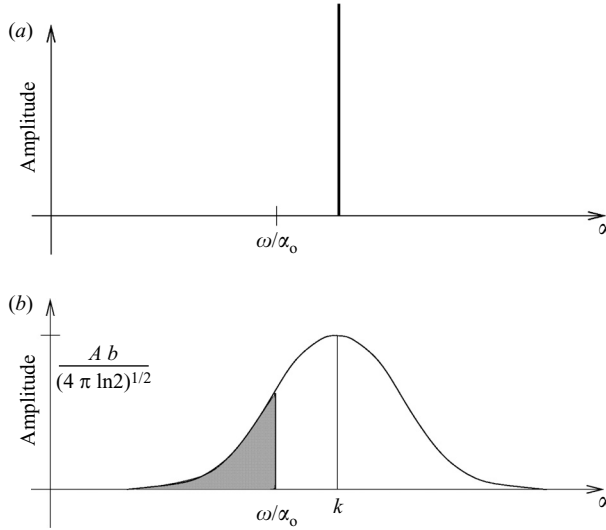
FIGURE 5. Wavenumber spectra. (*a*) Line spectrum of a constant-amplitude wave with a single wavenumber. (*b*) Broadband spectrum arising from wave-amplitude variation. Shaded region contains waves with supersonic phase velocity.

waves is important to noise generation. The significance of wave-amplitude growth and decay may best be seen by considering a pressure wave in a jet with angular frequency $\omega$, wavenumber $k$ and amplitude $A$. Mathematically, such a wave may be written in the form

$$p = A e^{i(kx-\omega t)}, \tag{1}$$

(only the real part is of interest to us). Such a constant amplitude wave behaves like a wavy wall. If the phase velocity $\omega/k$ is supersonic relative to ambient sound speed $a_0$, there will be Mach wave radiation. However, if the phase velocity is subsonic, there is no sound radiation. Now, if the wave amplitude undergoes growth and decay, then the wave no longer has just a single wavenumber $k$. Instead, the wave has a broadband of wavenumbers. For illustration purposes, suppose $A(x)$ is a Gaussian function with a half-width $b$ centred at $x_0$; i.e.

$$A(x) = A_0 e^{-(\ln 2)((x-x_0)/b)^2}. \tag{2}$$

Now, on replacing $A$ by $A(x)$ in (1), it is easy to find,

$$p(x,t) = A_0 e^{-(\ln 2)((x-x_0)/b)^2 + i(kx-\omega t)}$$

$$= \frac{A_0 b}{(4\pi \ln 2)^{1/2}} \int_{-\infty}^{\infty} e^{-(\alpha-k)^2 b^2/4\ln 2 + i(\alpha x - \omega t) + i(k-\alpha)x_0} \, d\alpha. \tag{3}$$

Equation (3) shows that the wave no longer has only one wavenumber $k$; it is now broadband (figure 5b). The spectrum has a Gaussian shape centred at $\alpha = k$. Suppose the original constant-amplitude wave is subsonic; that is $\omega/k < a_0$. In this case, the constant-amplitude wave will radiate no sound; but, with amplitude variation, a part of the spectrum could have phase velocity with $\omega/\alpha > a_0$ or supersonic phase velocity. This part of the spectrum (shaded in figure 5) will radiate sound. This is the mechanism by which large turbulence structures/instability waves of high subsonic jets radiate sound to the far field, as first suggested by Tam & Burton. Kopiev *et al.*

(2006) succeeded in measuring instability waves in a supersonic jet and its radiated noise. Their experiment offers a direct validation of the above instability-wave noise-generation mechanism.

Both the large turbulence structures and fine-scale turbulence of a jet radiate sound in the downstream direction. However, for high-speed jets, the large turbulence structures noise is, by far, the more intense. As a result, the measured data have a peaky spectrum figure 3.

In a recent series of two-point space–time correlation experiments, Panda & Seasholtz (2002) and Panda, Seasholtz & Elam (2005) appear to have provided the most direct evidence that there are two sources of jet noise. They used a technique based on Rayleigh scattering to measure the turbulent velocity and density fluctuations in a very localized volume (almost point-like measurements) inside a jet. They correlated this signal with the acoustic pressure measured by a far-field microphone to determine the source of noise. They found significant normalized correlations for point-like measurements at the end of the potential core of the jet and far-field microphone at 150°. The normalized correlations for jets at Mach number 1.8, 1.4 and 0.95 were 22 %, 19 %, and 7 %, respectively. These are substantial correlations. The correlations maintained at about the same level when the measurement point inside the jet was moved radially over the half-width of the jet and axially over a distance of a few jet diameters. On the other hand, when the far-field microphone was placed at 90°, the correlation dropped to the noise level of the facility (little correlation). Note that a far-field microphone receives noise from all sources in a jet. If the sources are small and localized, the correlation of far-field pressure with turbulence fluctuations of a small blob of turbulence (measured by the Rayleigh scattering technique) would be statistically insignificant. This is the case of noise radiated by fine-scale turbulence to the microphone at 90°. However, the strong correlation measured at 150° requires that the noise source be coherent over a sizeable volume. In this case, a considerable fraction of the noise received by the far-field microphone comes from the large coherent source. The experimental results of Panda *et al.* are consistent with the earlier observations of Hurdle, Meecham & Hodder (1974) and Schaffar (1979). In addition, the more recent correlation estimations by Bogey & Bailly (2005) using numerical simulation data computed by LES methodology also yielded very similar conclusions. Evidently, all these results are in support of the proposition that there are two noise sources in a high-speed jet. The dominant source that is responsible for radiation in the downstream direction is the large-scale turbulence whereas that in the sideline direction is the small-scale turbulence.

This investigation has two basic objectives. First, we would like to offer further experimental evidence to support the two-noise source model. Secondly, it is our intention to highlight some prominent characteristics of jet noise and noise sources. Four types of experimental data and results are presented in this paper.

1. Single microphone far-field noise data.
2. Two microphone far-field correlation data.
3. Rayleigh scattering jet turbulence measurements and far-field pressure correlation data.
4. Mirror microphone jet noise source distribution measurements.

The four types of experiment provide different insight into the jet noise radiation phenomenon. The first two types of measurement concentrate on the radiated sound field. The third experiment correlates source fluctuations with the radiated sound field. This may be regarded as a direct measurement of the noise source. The fourth experiment examines the noise source distribution inside a jet. These are distinct

| Experiment | Mach-number range | Range of temperature ratio ($T_r/T_a$) | Source of data |
|---|---|---|---|
| Single far-field microphone measurements | 0.3 to 2.0 | 1.0 to 3.2 | Seiner *et al.* (1992) Viswanathan (2004) Norum & Brown (1993) |
| Two far-field microphone correlation measurements | 0.9 and 1.67 | 1.0 and 3.2 | Present investigation |
| Direct correlation of turbulence fluctuations in jets and far-field microphone signal | 0.6 to 1.8 | 1.0 to 2.7 | Panda *et al.* (2005) and present investigation |
| Mirror microphone noise source distribution measurements | 0.5 to 1.9 | 1.0 to 3.2 | Present investigation |

TABLE 1. Experimental conditions and source of data.

experimental investigations. However, it will be shown that all four types of data and results are consistent with and in support of the two-noise source model of figure 4. Table 1 provides a summary of the experimental conditions of the four types of experiment in this investigation.

The rest of this paper is as follows. Sections 2 to 5 are independent sections. Each reports the measurements and results of one type of experiment as listed above. A conclusion in §6 completes this work.

## 2. Single-microphone far-field measurements

As a part of this investigation, we have examined and analysed a large collection of single-microphone far-field jet noise data. If, indeed, the measured data is from two sources as shown in figure 4 and they have very different characteristics, then it is reasonable to expect these characteristics to be imprinted on the radiated sound field. Thus, by analysing the far-field noise data systematically, it should be possible to show readily that there are two distinct sound fields. Once this is demonstrated, we would be able to infer what are some of the characteristics of the noise sources from those of the sound fields.

### 2.1. *Directivity*

If a turbulent jet has two noise sources, it is extremely unlikely that the noise directivities of the two sources have similar directional dependence. We would, therefore, anticipate the noise radiated from a jet to exhibit two distinct directional dependences. This can easily be verified by examining far-field microphone directivity data. Figure 6(*a*) shows a plot of the overall sound pressure level (OASPL), scaled to a distance of 100 fully expanded jet diameters, as a function of angle of radiation. The temperature ratio of the jets is 1.0 (cold jet). The data are taken from the measurements of Seiner *et al.* (1992) and Viswanathan (2004). In processing the data for this figure, measured noise spectra in the transitional directions are first decomposed into two components by means of the two similarity spectra as in figures 3(*d*) and 3(*e*). The OASPL of each noise component is then calculated. The solid circles of figure 6(*a*) are those of the broad peak spectrum (fine-scale turbulence noise). The open circles are those of the peaky spectrum (large turbulence structure noise). This figure shows
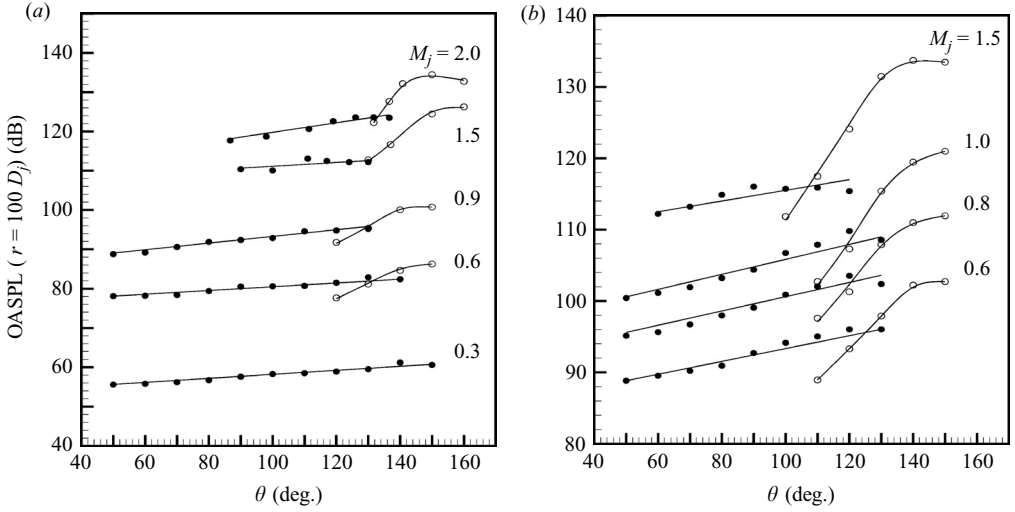
FIGURE 6. Variation of OASPL with inlet angle. (*a*) $T_r/T_a = 1.0$, (*b*) $T_r/T_a = 2.2$.

clearly that the large turbulence structure noise is highly directional and drops off rapidly around $\theta = 120°$ to $140°$. This characteristic is consistent with Mach wave radiation with a sharp cut-off around the Mach wave angle. The fine-scale turbulence noise increases gradually with $\theta$. This mild increase in the downstream direction is most probably the result of a source convection effect.

Figure 6(*b*) is a similar plot, but the jets are at a temperature ratio 2.2. At a fixed Mach number, the exit velocity is higher for a hotter jet. As a result, we would expect stronger Mach wave radiation for jets at a high temperature. This increase in noise radiation with jet temperature can easily be seen by comparing figures 6(*a*) and 6(*b*). Also, for the same reason, the disparity in the noise intensity radiated by the large turbulence structures and that by the fine-scale turbulence becomes larger for hot jets. This is very obvious in figure 6(*b*). This becomes even more prominent at higher jet Mach numbers and higher temperature ratios.

### 2.2. *Peak Strouhal numbers*

In the above subsection, the noise directivity was studied in the belief that if there were two noise sources in a jet they should exhibit different directional dependence. It is not difficult to see that the same reasoning also applies to the Strouhal number at the peak of measured noise spectrum. We will refer to this Strouhal number as the peak Strouhal number. Figure 7(*a*) shows the dependence of the measured peak Strouhal number, $St_{peak} = f_p D_j / u_j$ (where $f_p$ is the frequency at the spectrum peak), on the direction of radiation for Mach 0.6 jets at temperature ratios of 1.0, 1.8 and 2.7. In directions for which fine-scale turbulence noise is dominant, $St_{peak}$ increases slowly with angle $\theta$. Cold jets have high peak Strouhal numbers. In directions for which large turbulence structure noise dominates, the trend is totally different. The peak Strouhal number decreases rapidly with increase in $\theta$. Also the peak Strouhal number appears to be insensitive to jet temperatures.

Figure 7(*b*) shows similar peak Strouhal-number dependence on direction of radiation for Mach 1.0 jets at temperature ratios of 1.0, 2.2 and 3.2. On comparing figures 7(*a*) and 7(*b*), it becomes clear that for fine-scale turbulence noise, the peak Strouhal number is slightly higher for lower-Mach-number jets. However, for large
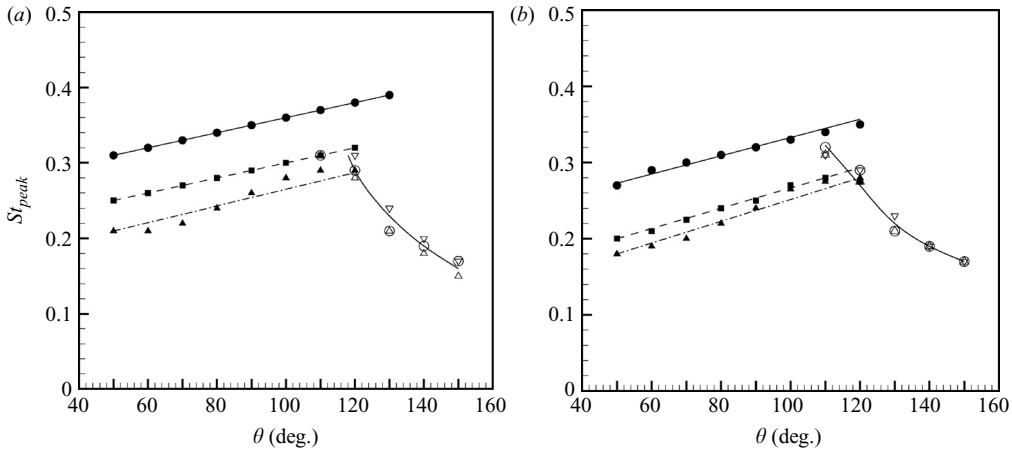
FIGURE 7. Variation of peak Strouhal number with inlet angle. (*a*) $M_j = 0.6$; ●, ▽, $T_r/T_a = 1.0$, ■, ○, $T_r/T_a = 1.8$, ▲, △, $T_r/T_a = 2.7$. (*b*) $M_j = 1.0$; ○, ▽, $T_r/T_a = 1.0$, ■, ○, $T_r/T_a = 2.2$, ▲, △, $T_r/T_a = 3.2$.

turbulence structure noise, the peak Strouhal number is relatively Mach-number and temperature independent. The distinctly different dependence of peak Strouhal number on direction of radiation as shown in figure 7 leaves little doubt that there are two very different sound fields surrounding a high-speed jet, suggesting that there must be two noise sources with greatly different characteristics.

### 2.3. *Power law*

It has been known since the early days of jet noise research that OASPL, $I$, of a jet varies as a high power of jet exit velocity. The most famous power law is the $u^8$ law of Lighthill. That is,

$$I \propto u^8. \tag{4}$$

However, based on his extensive jet noise data analysis, Viswanathan (2004, 2006) showed that his data fitted a generalized power law of the form,

$$I \propto u^n. \tag{5}$$

The exponent $n$ was determined empirically by him. Tam (2006) pointed out that a power law should be written in a dimensionless form. He further showed how the generalized power law might be derived as an approximation through dimensional analysis. Here, for completeness, a brief derivation of the power law is presented below.

Consider a jet noise experiment. There are two sets of input variables. The ambient gas variables are ($p_\infty$, $\rho_\infty$, $T_\infty$). The fully expanded jet flow variables are ($u_j$, $p_j$, $\rho_j$ and $T_j$). In addition we have two other variables, $\nu$ (the kinematic viscosity) and $D_j$ (the fully expanded jet diameter). However, because of the equation of state, $\rho_\infty$ and $\rho_j$ are not independent variables. Also upon invoking boundary-layer arguments (confirmed experimentally), $p_j$ is nearly equal to $p_\infty$. Thus, the six independent input variables are,

$$
\begin{array}{cccccc}
p_\infty, & a_\infty, & u_j, & T_r, & \nu, & D_j \\
\dfrac{M}{LT^3} & \dfrac{L}{T} & \dfrac{L}{T} & \dfrac{L^2}{T^2 R} & \dfrac{L^2}{T} & L
\end{array},
$$

where we have used $a_\infty$, the ambient sound speed instead of $T_\infty$ and $T_r$, the reservoir or total temperature of the gas of the jet, instead of $T_j$. The latter is possible because $T_j$ is related to $T_r$ and $u_j$ by the nozzle flow energy equation. The dimensions of each of these variables in terms of the fundamental dimensions $L$ (length), $T$ (time) and $M$ (mass) are given below each variable. Also $R$ is the gas constant. Note that $p_\infty$ is the only variable with a dimension of $M$, so it cannot form a dimensionless group with other input variables. Three-dimensionless groups can be formed from the remaining variables. A convenient choice of dimensionless groupings is

$$\frac{u_j}{a_\infty}, \frac{T_r}{T_\infty}, \frac{u_j D}{\nu} = Re \quad \text{(Reynolds number of the jet)}.$$

Let $I(r, \theta)$ be the OASPL of jet noise measured at an observation point with spherical polar coordinates $(r, \theta', \phi)$. The coordinate system is centred at the nozzle exit with the polar axis in the direction of jet flow. $\theta'$ is equal to $180° - \theta$. $\theta$ is the inlet angle which is used throughout this work. $I(r, \theta)$ has dimensions of $p_\infty^2$. Therefore, by the Buckingham $\pi$-theorem, we may write,

$$\frac{I(r, \theta)}{p_\infty^2} = \frac{K\left(\dfrac{u_j}{a_\infty}, \dfrac{T_r}{T_\infty}, Re, \theta\right)}{\left(\dfrac{r}{D_j}\right)^2}, \tag{6}$$

where $K$ is yet an unknown function. We have incorporated the inverse squared $r$-dependence of far-field sound in formula (6). For high-Reynolds-number jets, $Re$ is not a sensitive parameter and may be omitted. The generalized power law is obtained by approximating the function $K[(u_j/(a_\infty)), (T_r/T_\infty), \theta]$ by a power function of $u_j/a_\infty$. This leads to,

$$\frac{I(r, \theta)}{p_\infty^2} = A \frac{\left(\dfrac{u_j}{a_\infty}\right)^n}{\left(\dfrac{r}{D_j}\right)^2}. \tag{7}$$

The power law exponent $n$ and proportionality factor $A$ are both dependent on $\theta$ and $(T_r/T_\infty)$.

The generalized power law (7) is an empirical law. Its validity has been verified experimentally (see Tam 2006). We will now present data to show it is, indeed, a good approximation. Figure 8(a) is a log–log plot of the quantity on the left-hand side of (7) versus $(u_j/a_\infty)$, scaled to $r/D_j = 100$ for noise radiated in the 90° direction at five temperature ratios. As can be seen, each set of data lies on a straight line, confirming that $I/p_\infty^2$ varies as a power function of $(u_j/a_\infty)$. Figure 8(b) shows a similar plot for noise radiated in the 150° direction. Again, each set of data lies approximately on a straight line. By measuring the slope of each straight line and its intercept at $(u_j/a_\infty) = 1$, the velocity exponent $n(\theta, T_r/T_\infty)$ and the proportionality factor $A(\theta, T_r/T_\infty)$ of generalized power law (7) can be easily determined.

Now, if there are two noise sources in a high-speed jet as depicted in figure 4, it is highly unlikely that the power-law dependence of the large turbulence structure noise and that of the fine-scale turbulence noise would be similar. Thus, by plotting the power-law exponent $n$ and the proportionality factor $A$ as functions of direction $\theta$ at a fixed temperature ratio, we expect to see clear differences. Figure 9(a) shows the variation of power-law exponent $n$ as a function of $\theta$ for $(T_r/T_\infty) = 1.0$. This figure
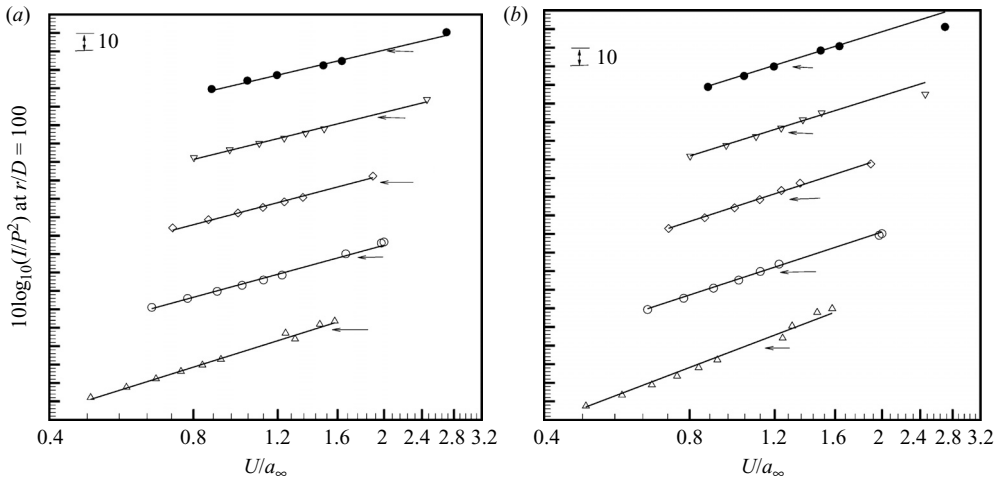
FIGURE 8. Variation of OASPL with jet acoustic Mach number. (*a*) Inlet angle 90°. (*b*) Inlet angle 150° ← vertical axis equal to −80.0 for the curve. ●, $T_r/T_a = 1.0$; ▽, 1.8; ◇, 2.2; ○, 2.7; △, 3.2.
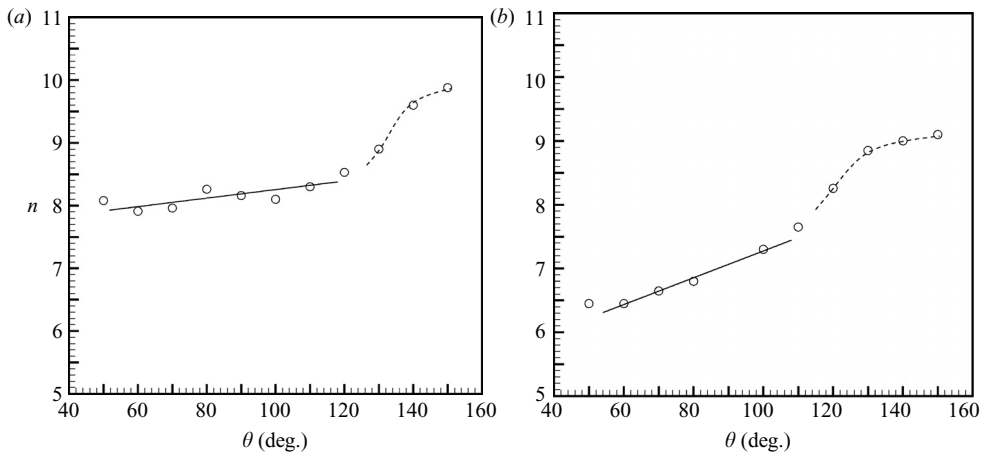


FIGURE 9. Variation of power-law exponent $n$ with inlet angle. (*a*) $T_r/T_a = 1.0$.
(*b*). $T_r/T_a = 2.7$.

exhibits two distinct dependences of $n$ on $\theta$. In the sector $\theta < 120°$ for which fine-scale turbulence is dominant, $n$ varies only a little with $\theta$. $n$ is approximately equal to 8, which is in agreement with Lighthill's $u^8$ law. In the downstream sector $\theta > 120°$, there is a rapid increase in $n$ with $\theta$. As $\theta$ approaches 150°, $n$ approaches 9.9. This is the sector dominated by the large turbulence structure noise. The power-law exponent for this noise is significantly larger than 8. Figure 9(*b*) shows the variation of $n$ with respect to $\theta$ for jets at a temperature ratio of 2.7. Again, there are two distinct dependences of $n$ on $\theta$. It is worth pointing out that for hot jets, $n$ is usually smaller than 8. In fact, figure 10(*b*) indicates that it is as small as 5.5 for $\theta = 60°$. Generally speaking, Lighthill's $u^8$ law is not valid for hot jets.

Figure 10(*a*) shows the dependence of proportionality factor $A$ on $\theta$ for cold jets. It is obvious that there are two distinct directional dependences. One is for $\theta < 120°$
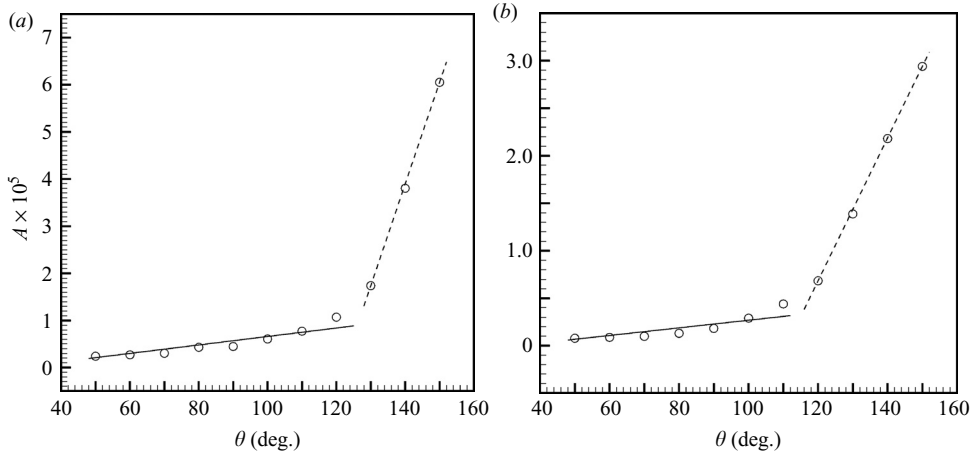
FIGURE 10. Variation of power-law multiplicative factor A with inlet angle.
(a) $T_r/T_a = 1.0$. (b) $T_r/T_a = 2.7$.

and the other for $\theta > 120°$. This is consistent with the change in dependence of $n$ on $\theta$ shown in figure 9(a). Figure 10(b) shows a similar plot, but for hot jets at temperature ratio 2.7. Again, the figure shows two distinctly different behaviours of $A(\theta, T_r/T_\infty)$. The change in dependence of $A$ on $\theta$ is consistent with figure 9(b).

   In summary, the power-law data provide clear evidence that there are two sound fields associated with a high-speed jet. These two sound fields are so distinctly different that they can only be generated by two vastly different sources in the jet. This conclusion is consistent and supportive of the two-noise sources model of figure 4.

## 2.4. *Noise spectra of low-Mach-number jets*

One simple way to demonstrate that one of the noise components of a jet is Mach wave radiation from the large turbulence structures is to eliminate or suppress those structures in the jet flow and examine the resulting changes in the measured noise spectra. In the absence of large turbulence structures, the sound field of a jet will have a broad peak noise spectrum, as shown in figure 3(a), in all directions. Such a demonstration was carried out by Tam & Zaman (2000). In one of their jet noise experiments, a six-lobe nozzle was used. The narrowness of the nozzle effectively prevented the formation of large turbulence structures in the jet flow. The radiated noise was primarily from the fine-scale turbulence; this was confirmed by comparing the shape of the measured noise spectra in all directions, including those in the downstream direction close to the jet axis, with the broad peak similarity spectrum of figure 2. There was good agreement in every comparison. Here, a similar demonstration is presented by considering the noise from low-Mach-number jets.

   As the jet Mach number reduces, Mach wave radiation becomes inefficient and ineffective. At sufficiently low Mach number, the part of the wavenumber spectrum of the large turbulence structures of a jet that has supersonic phase velocity relative to ambient speed of sound shrinks dramatically (see figure 5b). Thus the fine-scale turbulence noise becomes the dominant component even in directions close to the jet axis. Figure 11 shows the noise spectra of a Mach 0.3 cold jet measured by Norum & Brown (1993) (these are data measured as a part of their published work and are made available to the present investigation). Six spectra are shown at every
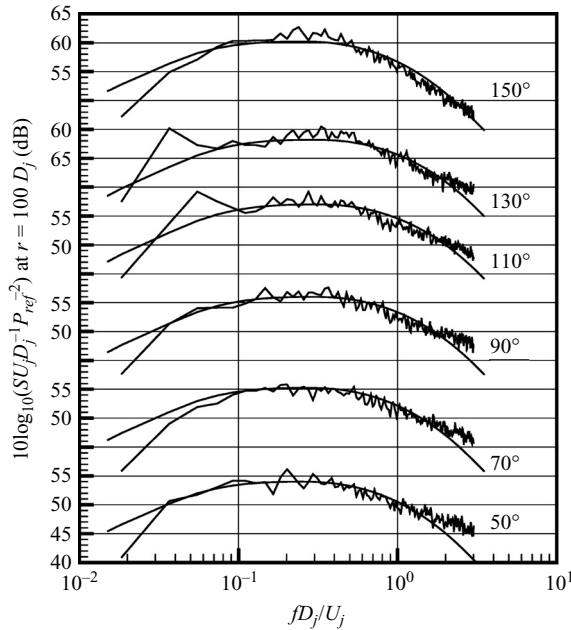
FIGURE 11. Comparisons of measured spectra with the broad peak similarity spectrum. Jet Mach number $= 0.3$, $T_r/T_a = 1.0$.

$20°$ interval from inlet angle $50°$ to $150°$. The smooth curve is the similarity spectrum. Clearly, the broad peak similarity spectrum of figure 2 is a reasonably good fit to the entire set of data. We believe the Norum & Brown data of figure 11 together with the six-lobe nozzle experiment of Tam & Zaman demonstrate convincingly that it is possible to suppress one source of noise in order to expose the acoustic radiation of the other source. This can be done, of course, only if a jet has two noise sources. Therefore, the data of figure 11 does provide an indirect confirmation that high-speed jets have two independent noise sources. We would like to add that Viswanathan (2007) reported the observation of jet noise spectra that fitted the peaky spectrum of figure 2 for low-Mach-number jets at inlet angles larger than $150°$.

## 3. Two-microphone far-field correlation measurements

Maestrello (1976) was one of the first to study jet noise using two-microphone far-field data. However, his investigation was confined to subsonic jets. Maestrello's stated objective was to use two-microphone far-field measurements to deduce the equivalent acoustic sources in a jet by solving an 'inverse problem'. His equivalent sources were the Lighthill quadrupoles. In the present work, both subsonic and supersonic jet noise data are measured. Our objectives are very different from Maestrello's; we aim to use the correlation data to investigate the spatial structure and characteristics of the radiation field. By spatial structure, we mean the coherence of the sound field in the radial as well as in the polar angle direction. We will use the observed properties and characteristics of the sound field, to infer what the noise sources and their characteristics are. Specifically, we will offer strong evidence that the inferred noise sources are consistent with the two-noise source model of figure 4.
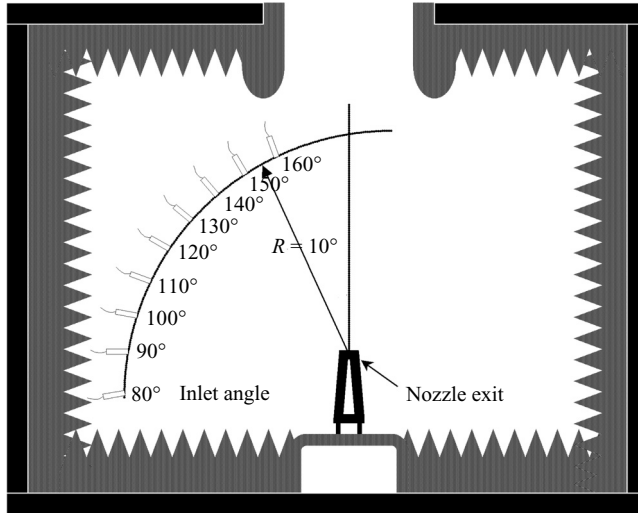
FIGURE 12. Schematic diagram showing the microphone set-up on a polar arc in the GTRI anechoic chamber.
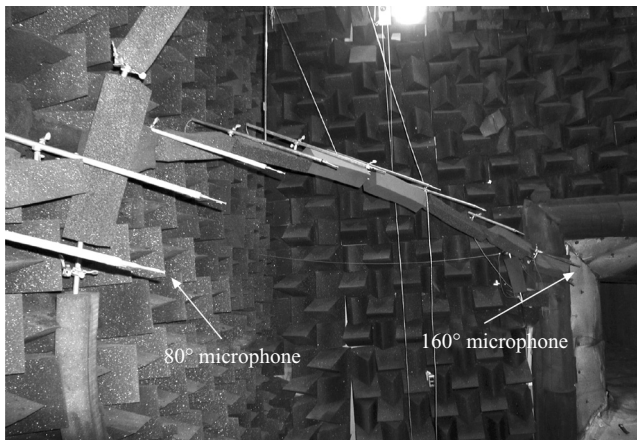


FIGURE 13. Photograph of the microphone array in the GTRI anechoic chamber.

### 3.1. *Experimental set-up*

Two-microphone correlation measurements were carried out at the Georgia Tech Research Institute static anechoic chamber. A convergent nozzle of 1.6 in exit diameter was used for the subsonic Mach 0.9 jet experiment. A 2 in diameter convergent–divergent nozzle was used for the supersonic Mach 1.67 jet experiment. The data acquisition settings were as follows: $\Delta f = 24\,\mathrm{Hz}$, frequency span from 0 to 76.8 kHz, 512 averages, 25 % overlap. Figure 12 is a schematic diagram of the microphone array set-up inside the anechoic chamber (not to scale). The microphones were mounted on an arc at a distance of 10 feet from the nozzle exit. They were placed 10° apart from $\theta = 80°$ to 160°. A photograph of the microphones inside the anechoic chamber is shown in figure 13.

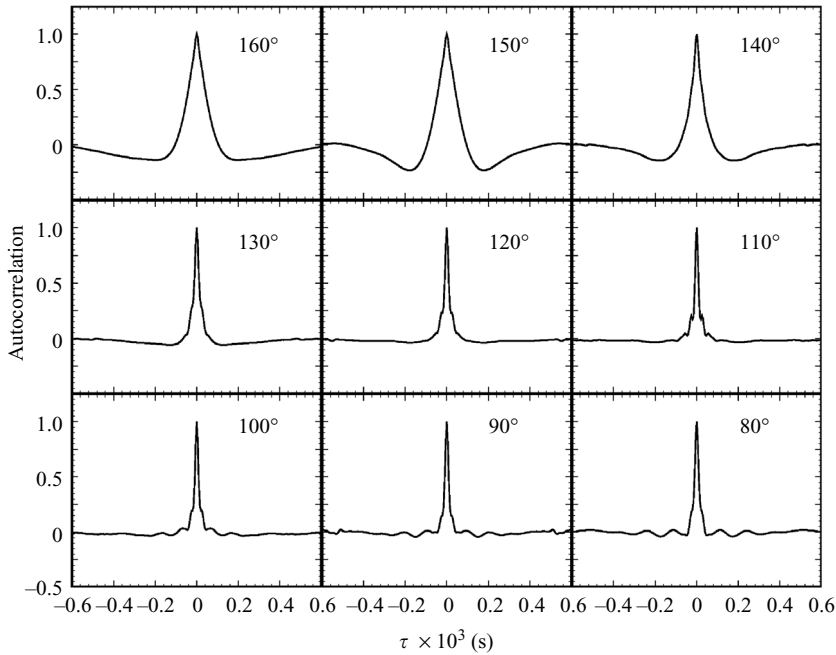FIGURE 14. Normalized autocorrelations of a supersonic jet at Mach 1.67.

### 3.2. *Autocorrelation measurements*

Let $p_n(t)$ be the pressure–time signal measured by the $n$th microphone. The normalized autocorrelation, $R_{nn}(\tau)$, is defined as,

$$R_{nn}(\tau) = \frac{\langle p_n(t)p_n(t+\tau)\rangle}{\langle p_n^2(t)\rangle}. \tag{8}$$

In (8), $\langle\ \rangle$ means ensemble or time average (the two are equivalent as the noise field is stationary random).

Autocorrelation function provides a time scale of coherence of the sound field. By appealing to the fact that acoustic waves propagate at the speed of sound, it is possible to convert the correlation time to a spatial correlation length. This offers a measure of the coherence of the sound field in the radial direction (direction of radiation). The sound field generated by the large turbulence structures of a jet should be quite different from the sound field generated by the fine-scale turbulence. We, therefore, expect the normalized autocorrelation to exhibit distinct differences depending on whether or not the microphone is placed inside the Mach wave radiation cone of figure 4. Figure 14 shows the measured normalized autocorrelations for the Mach 1.67 jet at nine microphone positions. It is easily seen that the autocorrelations form two distinct sets, each with a characteristic shape. Those at $\theta = 160°$, $150°$ and $140°$ are alike, while the shapes of the autocorrelations at all the other angles belong to a different set. This observation suggests that the jet, indeed, generates two very different noise fields; consistent with the noise spectrum data examined earlier. This may not be too surprising, however. Autocorrelation function is merely the Fourier transform of the noise spectrum. In §1, it was shown that jet noise spectra have two fundamental shapes, so it is natural that the autocorrelations also exhibit two distinct shapes. Figure 15 shows the autocorrelations of the Mach 0.9 jet. The shapes
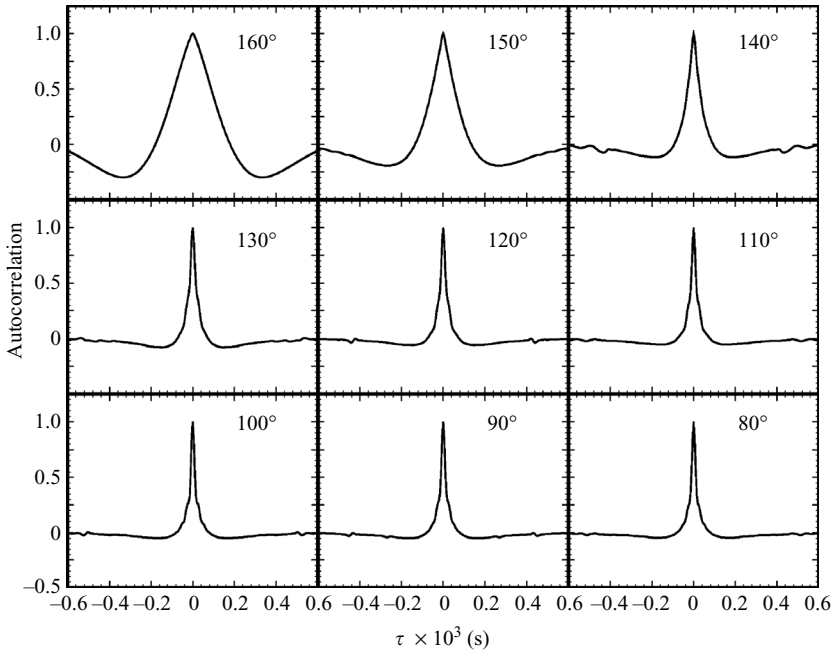
FIGURE 15. Normalized autocorrelations of a subsonic jet at Mach 0.9.

of the autocorrelations are very similar to those of figure 14. Note: in figure 14 the minor wiggles in the autocorrelations at angles 80°, 90° and 100° are the results of low-amplitude reflections from the walls of the anechoic chamber. They should be ignored.

A normalized autocorrelation offers a useful measure of the coherence of a random signal. At delay time $\tau = 0$, the normalized autocorrelation is equal to unity by definition. Now if the signal is totally random, then even for a small $\tau$, the time-delayed signal $p(t + \tau)$ has an equal probability of being positive or negative. Thus, the time average of the product $p(t)\, p(t + \tau)$ will be zero. For such a signal, the normalized autocorrelation drops quickly from one to zero over a very small $\tau$.

We may view the sound field of a jet as consisting of random pulses or packets of pulses. A train of acoustic waves may be regarded as a series of pulses linked together. An acoustic pulse has a spatial dimension or size. Suppose the size of a typical pulse is $\lambda$. If $\lambda$ is very small, then the normalized autocorrelation of such an acoustic field would have the shape of a spike with a very narrow half-width. This is because for time delay $\tau > \lambda/a_0$ ($a_0$ is the speed of sound), the signal is random and uncorrelated. It is reasonable to expect the size of the acoustic pulses from fine-scale turbulence to be small; probably the same size as the energetic turbulent eddies. For this reason, the normalized autocorrelation measured in the sideline directions of the jet is expected to have narrow half-widths. It is also reasonable to expect the size of the acoustic pulses or packets of pulses radiated by the large turbulence structures to be much larger; say, similar size to that of the large turbulence structures. Hence the half-width of the normalized autocorrelations measured within the Mach wave radiation cone of figure 4 would be correspondingly wider. This is obviously true, as shown in figures 14 and 15.
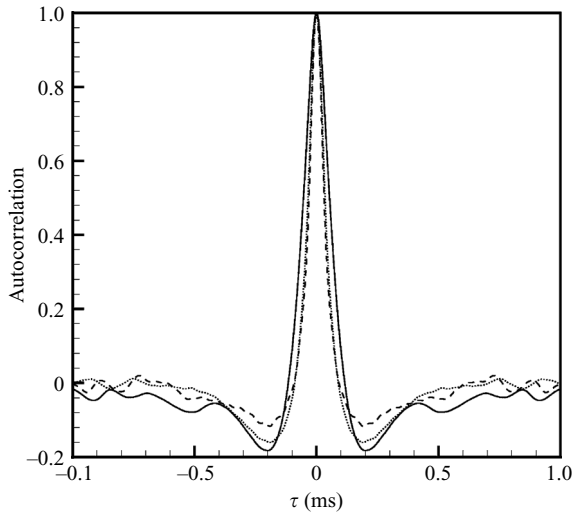
FIGURE 16. Autocorrelation of a Mach 0.9 jet at a temperature ratio of 3.2.
————, 150°; · · ·, 120°; – – –, 90°.

Figure 16 shows a comparison of the autocorrelation functions measured at 90°, 120° and 150° for a Mach 0.9 jet at a temperature ratio of 3.2. The 90° autocorrelation function is a good representation of that of the fine-scale turbulence noise. The 150° autocorrelation function is a good representation of that of the large turbulence structure noise. In addition to that, the half-widths of the two functions are distinctly different, the autocorrelation of the large turbulence structure noise is characterized by very large and deep negative peaks; twice as deep as that of the fine-scale turbulence noise. The 120° autocorrelation function is almost the same as the 90° function except for the negative peaks. Figure 3(*e*) shows the noise spectra of jets at 120° angle. At high subsonic Mach number, the noise spectrum is made up primarily of the contributions from fine-scale turbulence noise. However, there is also a peak component due to the large turbulence structures. This observation suggests that the first effect of the presence of large turbulence structure noise is the deepening of the negative peaks in the autocorrelation function.

Figure 17 shows an enlarged normalized autocorrelation function of the Mach 1.67 jet at 150°. As pointed out above, one prominent feature of this function is the large negative peaks. They are an intrinsic characteristic of large turbulence structure noise. The reason why there are large negative peaks is not difficult to understand. Figure 18(*a*) shows a basic large acoustic pulse with a compression phase (positive pressure above the mean) and an expansion phase (negative pressure). In this figure, the compression phase of the pulse is assumed to be ahead of the expansion phase. The arguments presented below, however, are independent whether the compression or expansion phase is ahead. Figure 18(*a*) represents a typical measured acoustic pulse from the large turbulence structures. Figure 18(*b*) and 18(*c*) show the pulse as time advanced and delayed by an interval $\tau$. The products $p(t)p(t+\tau)$ and $p(t)p(t-\tau)$ are obviously negative and are near the most negative values. Further increase in $\tau$ will cause the products to become zero eventually. This explains why the normalized autocorrelation of the large turbulence structure noise should start at 1.0 at $\tau = 0$ and drops to a negative value as $\tau$ increases. It will reach a maximum negative value before approaching zero at large $\tau$. Figure 18 suggests that a good measure of the
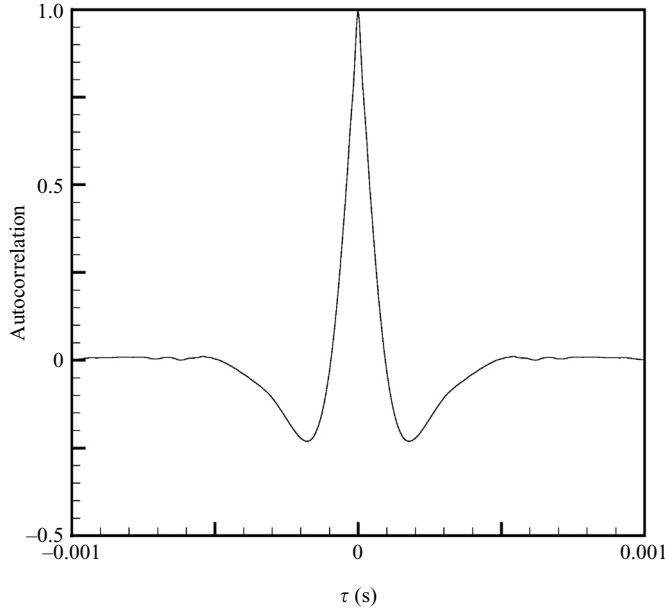
FIGURE 17. Normalized autocorrelation at $\theta = 150°$, Mach 1.67 jet.
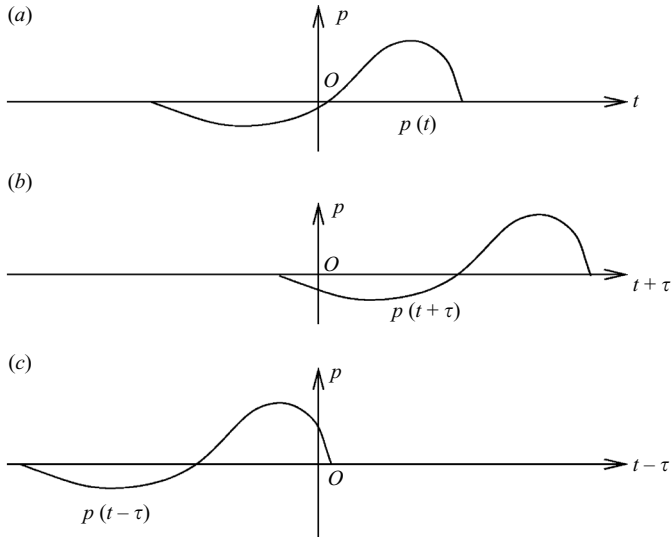


FIGURE 18. Values of $\pm\tau$ for which the autocorrelation function is negative.

coherence time of the large acoustic pulses from the large turbulence structures of the jet is around twice the correlation time at which the autocorrelation function reaches its maximum negative value. In figure 17, the maximum negative value occurs at $\tau_{neg\,max} = 1.8 \times 10^{-4}$ s. If $\lambda_{corr}$ is the spatial correlation length of the acoustic field in the radial direction, then $\lambda_{corr}$ is related to $\tau_{neg\,max}$ by,

$$\lambda_{corr} \cong 2\tau_{neg\,max} a_0. \qquad (9)$$

This yields $\lambda_{corr} \cong 2.4\ D_j$. Since acoustic waves are non-dispersive, this correlation length applies to the sound field, independent of the distance from the jet until it
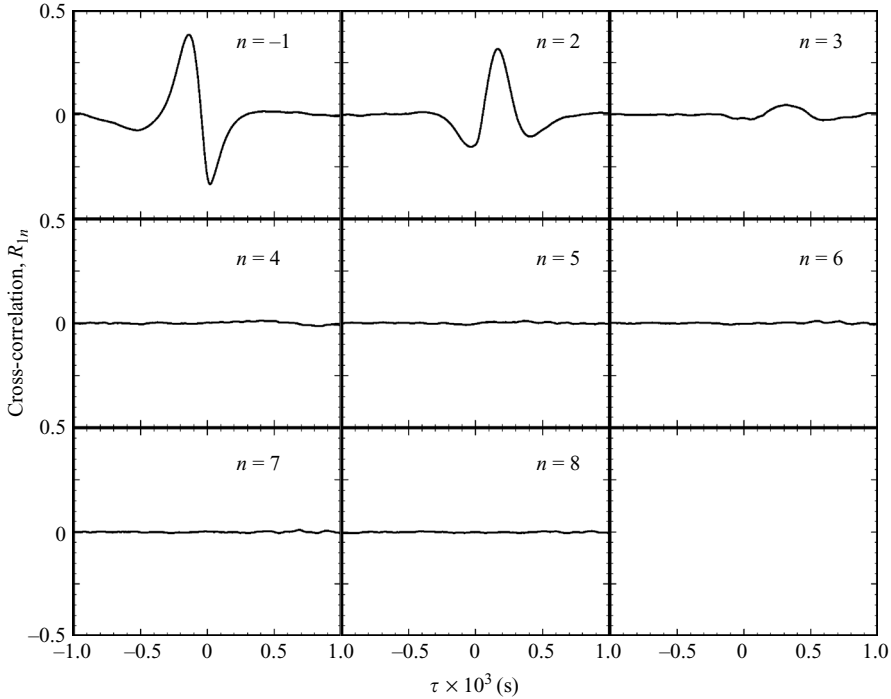
FIGURE 19. Cross-correlation with a fixed microphone at $\theta = 150°$, Mach 1.67 jet.

is far enough that viscous effect has time to influence the acoustic waveform. This reasoning leads us to believe this is also a measure of the spatial coherence of the noise source.

### 3.3. *Cross-correlation measurements*

To obtain spatial information on the structure of the sound field of a jet in the polar angle direction, microphone pressure cross-correlations were measured for both the Mach 0.9 and 1.67 jets. For convenience, we will refer to the microphones at $\theta = 150°$, $140°, \ldots, 80°$ as the first, second, $\ldots$, eighth microphone (see figure 12). As in the case of normalized autocorrelation measurements, we expect the cross-correlation data to exhibit two distinct angular dependences depending on whether the microphones are inside or outside the Mach wave radiation cone of figure 4. If $p_m(t)$ is the pressure-time signal of the $m$th microphone and $p_n(t)$ is that of the $n$th microphone, then the normalized cross-correlation, $R_{mn}(\tau)$, is defined as,

$$R_{mn}(\tau) = \frac{\langle p_m(t)p_n(t+\tau)\rangle}{\langle p_m^2(t)\rangle^{1/2}\langle p_n^2(t)\rangle^{1/2}}. \tag{10}$$

Figure 19 shows the measured normalized cross-correlation $R_{1n}(\tau), n = 2, 3, 4, \ldots, 8$. The $\theta = 150°$ microphone ($m = 1$) is the fixed microphone. $n = -1$ is the microphone at $\theta = 160°$. This figure serves to show not only the characteristic shape of the cross-correlation $R_{mn}(\tau)$, but also indicates the lack of correlation when the second microphones is outside the Mach wave radiation cone of figure 4. Unlike autocorrelation, cross-correlation is not a symmetric function of $\tau$. However, $R_{mn}(\tau)$ does have both positive and negative maxima. We will use the maximum value as an indicator of the coherence of the pressure signals at the two microphone positions.
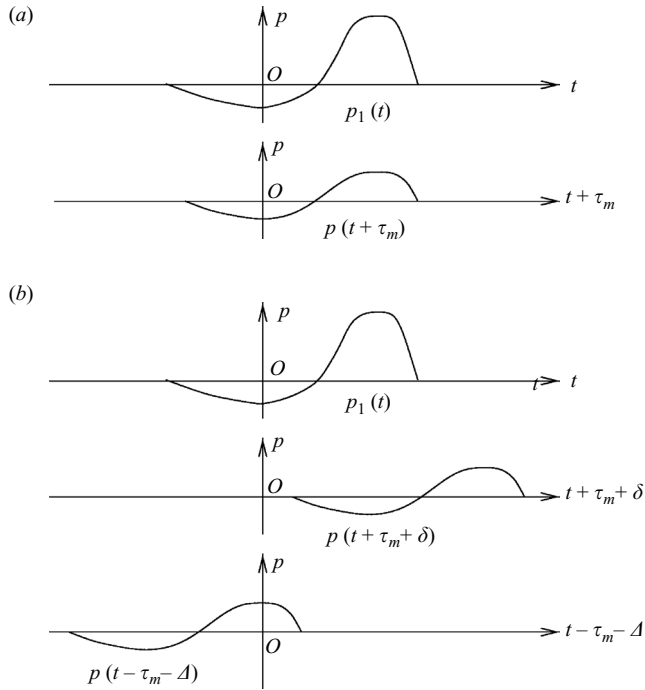
FIGURE 20. Cross-correlation at microphones 1 and 2. (*a*) Delay time $\tau_m$ for maximum positive Correlation. (*b*) Delay time $\tau_m + \Delta$ and advance time $\delta - \tau_m$ for maximum negative correlation.

The reason for the existence of positive and negative maxima is quite similar to the explanation given above for autocorrelation. Figure 20(*a*) shows the time histories of an acoustic pulse generated by the jet measured by two neighbouring microphones. The pressure signals are not identical, but similar. Thus, by delaying the time of $p_2$ by an appropriate time interval $\tau_m$, the signals $p_1$ and $p_2$ are aligned. Their product would have a positive maximum value. The time delay $\tau_m$ is required primarily because of the slight difference in propagating distance. Figure 20(*b*) shows that by further increasing the time delay by $\Delta$ or by advancing by $\delta$, the product of $p_1$ and $p_2$ is most negative. This will lead to a negative maximum in the cross-correlation.

Values of the maximum cross-correlations measured by the microphone array are plotted as bar charts in figure 21 (Mach 0.9 jets) and figure 22 (Mach 1.67 jets). An examination of these figures reveals that when both microphones are in the sector for which large turbulence structure noise is dominant ($\theta \geqslant 130°$), the maximum normalized cross-correlation can reach as high as 0.6. Outside this sector, the cross-correlation at 10° intervals is generally very low. The values are no more than 0.1, even for correlation with the immediate neighbour microphone. Beyond the immediate neighbour microphone, the correlation is extremely low. In many cases, it is within the noise level of the facility. These results indicate that the sound field radiated in the direction $\theta \geqslant 130°$ is fairly coherent, as expected of noise from large turbulent structures of the jet, whereas the sound field radiated outside this cone is poorly correlated in the polar angle direction, consistent with the expected characteristics of fine-scale turbulence noise.

Now let us examine the cross-correlation results further in the light of the two-noise source model of figure 4. In this model, the sound waves radiated to the sideline and
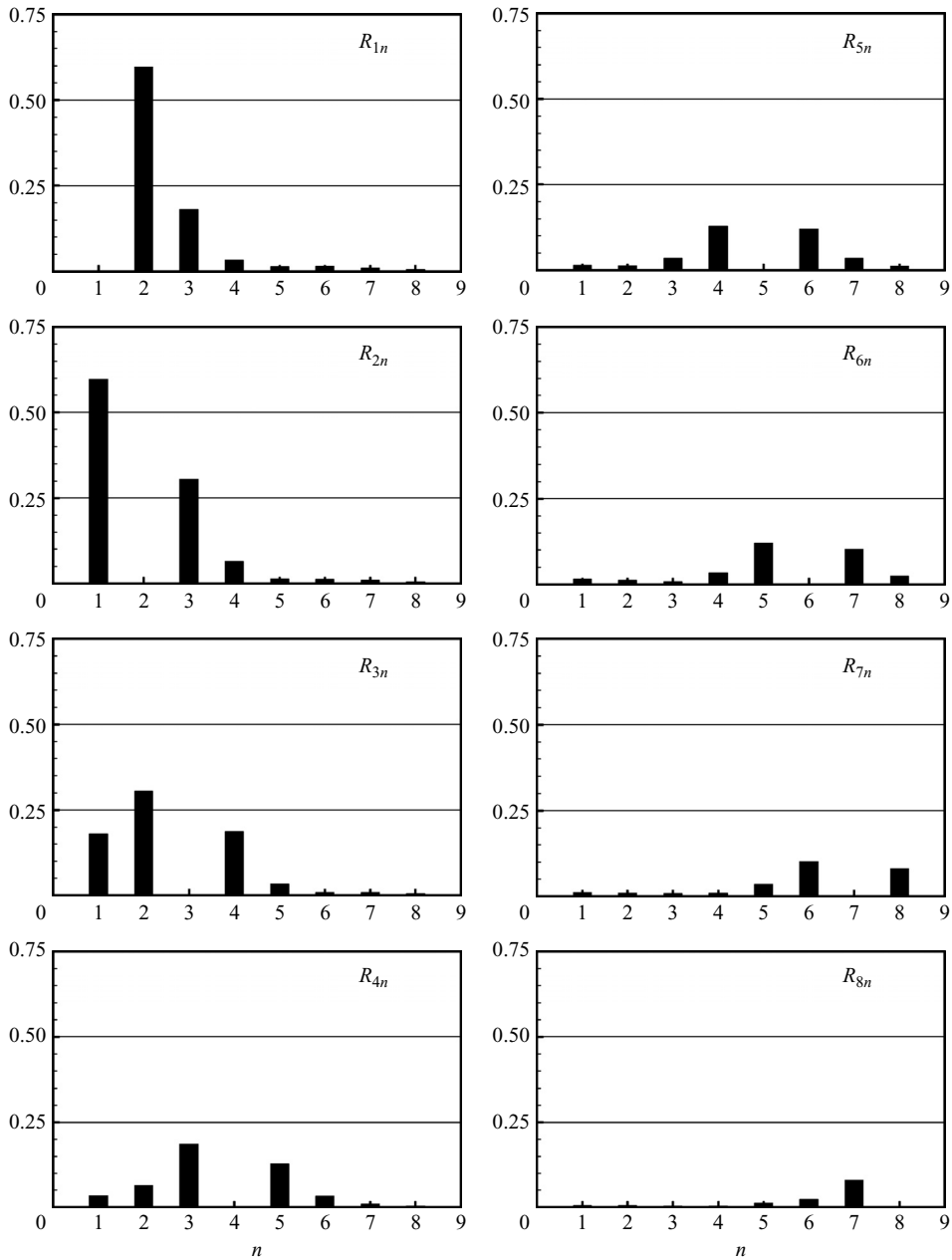
FIGURE 21. Bar chart showing maximum cross-correlation $R_{mn}$ for a Mach 0.9 jet.

in the upstream direction of the jet are from the fine-scale turbulence. The fine-scale turbulences are random and spatially uncorrelated. Thus, the sound field generated would consist of random pulses with narrow widths. The widths are of the order of the size of a typical blob of fine-scale turbulence. A sketch of the sound field near an array of far-field microphones arranged in a circular arc is shown in figure 23. Each acoustic pulse will impinge on the two microphones A and B at different times. Because the width of a sound pulse is small, the time during which a microphone
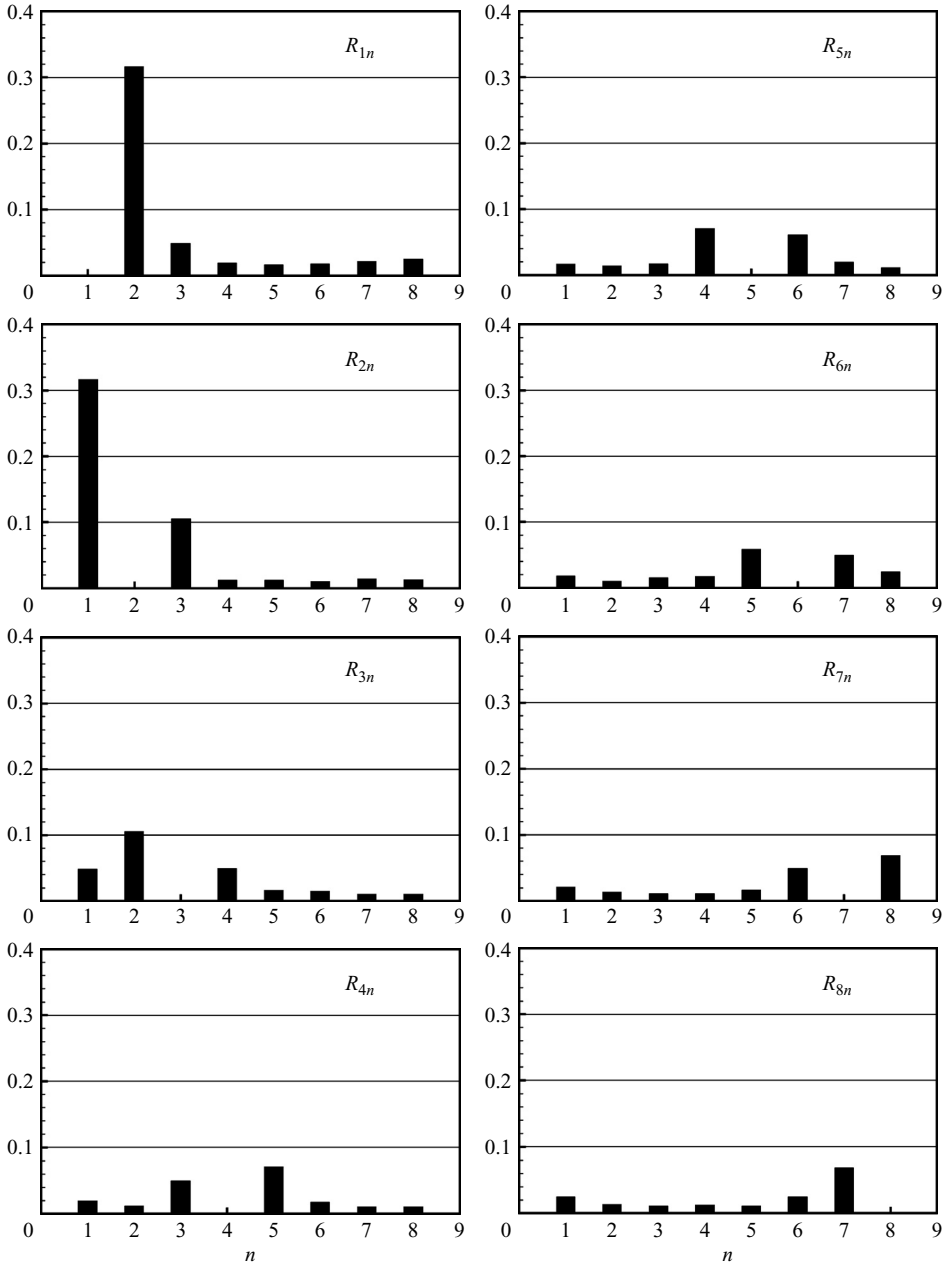
FIGURE 22. Bar chart showing maximum cross-correlation $R_{mn}$ for a Mach 1.67 jet.

registers a signal is short. This means that for the measured signal to contribute to the cross-correlation of microphones A and B at a prescribed time delay $\tau$, the pulse must strike the two microphones at a time difference of nearly $\tau$. The randomness of the sound field in figure 23 clearly suggests that this is not likely to happen very often. Thus, the normalized cross-correlation would be small. This is confirmed by the measured data in figures 21 and 22.
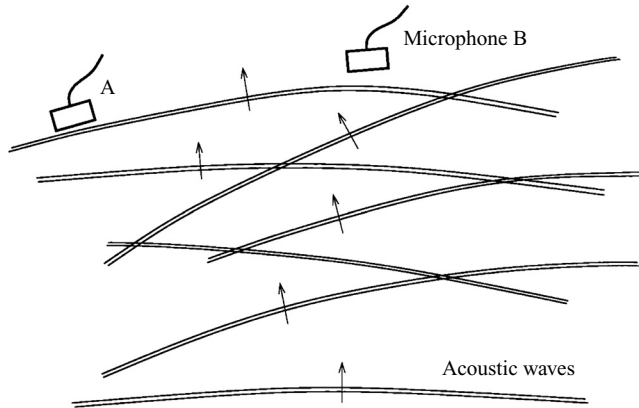
FIGURE 23. Sketch of the sound field from the fine-scale turbulence of a high-speed jet in the vicinity of a far-field microphone array.
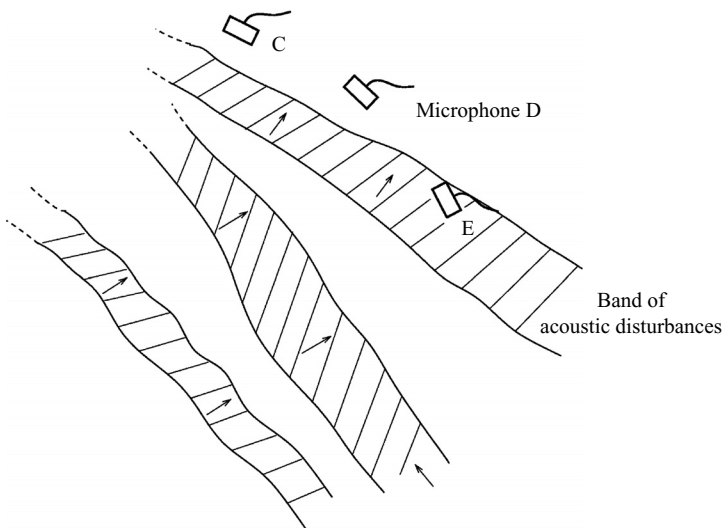


FIGURE 24. Sketch of the sound field from large turbulence structures of a high-speed jet in the vicinity of a far-field microphone array.

For the sound field in the downstream direction, the two-noise source model of figure 4 suggests that it is from the large turbulence structures. In the near field, just outside the jet flow, the radiated sound is in the form of Mach waves. However, when the sound waves propagate beyond the near field, they are no longer, strictly speaking, Mach waves, but simply outgoing sound waves. That is, they spread out in space so that the amplitude decreases inversely proportionally to the distance from the source in the same manner as all freely propagating sound waves. Here, the term 'Mach wave radiation' is used in a generalized sense. It is applied to sound waves that are generated originally as Mach waves, although they are no longer Mach waves in the far field. The acoustic pulses generated by the large turbulence structures of the jet flow have pulse widths of the order of the size of the large turbulence structures. Figure 24 shows a sketch of the sound field near a far-field microphone array. Because the widths of the pulses are substantial, the time during which a microphone senses

the pulse is long. This improves significantly the probability of two microphones, such as microphones D and E in figure 24, measuring the same pulse at a time difference of $\tau$. In this way, each sound pulse makes a contribution to the cross-correlation function. This results in substantial cross-correlation for these two microphones. This explains why there is considerable cross-correlation when two microphones are located in the downstream direction, as observed in the experimental measurements. The sound pulses of large turbulence structures are strongly directional. Microphone C in figure 24 is located outside the radiation zone. Therefore, the cross-correlation function between C and D and C and E is very small. This is in agreement with the measured normalized cross-correlation functions shown in figures 21 and 22. We would like to emphasize that the crucial difference between the characteristics of the normalized cross-correlation function of the sound field radiated by the fine-scale turbulence and that by the large turbulence structures of the jet flow is simply the width of the sound pulses. The intensity of sound plays a less significant role.

What emerges from the present far-field microphone correlation measurements is that the noise field of a high subsonic to moderately supersonic jet has a radial correlation length of about two jet diameters within the cone $\theta \geqslant 130°$. On a spherical surface in the acoustic far field, there is also significant correlation of the noise field within this cone in the polar angle direction. However, outside this cone, the noise field has only a very limited spatial correlation both radially and in the polar angle directions. These results are new. The cone angle $\theta \geqslant 130°$ is consistent with the angle at which there is a change in dominance between large turbulence structure noise and fine-scale turbulence noise for Mach number in the range of 0.9 to 2.0 as observed in the noise intensity data of figure 6(*a*) in §1. They provide a different perspective of the noise field of high-speed jets. Most importantly, these experimental observations are consistent and supportive of the two-noise source model of figure 4.

## 4. Direct correlation of jet turbulence fluctuations and far-field sound

Intuitively, the most direct way to determine the source of jet noise is to correlate turbulence fluctuations in a jet with far-field sound. Over the years, there have been a number of attempts to perform such direct measurements (e.g. Lee & Ribner 1972; Siddon 1973; Hurdle, Meecham & Hodder 1974; Schaffar 1979; Richarz 1980). Earlier works by Lee & Ribner, Siddon and Hurdle *et al.* used hot wire to measure turbulence velocity or microphone to measure *in situ* pressure fluctuations. Such data are not reliable as the insertion of a hot wire or a microphone into a jet leads to interference effects. More recent studies by Schaffar and Richarz used laser-Doppler velocimetry (LDV). This is an improvement over hot wire; however, LDV requires seeding particles as tracers. This creates new issues such as what size particles and the minimum particle density to use for accurate measurements. Seashotlz, Panda & Elam (2001, 2002) and Panda (2007) developed instruments for measuring density and velocity fluctuations in high-speed turbulent jets using a molecular Rayleigh scattering technique. This technique is based on the scattering of laser light by the gas molecules present in the jet. The advantage of this method is that there are no intrusive probes and it is free from particle seeding problems. Panda & Seasholtz (2002) and Panda *et al.* (2005) subsequently employed the Rayleigh-scattering technique to measure direct correlations between density and velocity fluctuations in turbulent high-speed jets and microphone sound pressure signals in the far field. We would like to point out that their works represent the first successful direct correlation measurements.
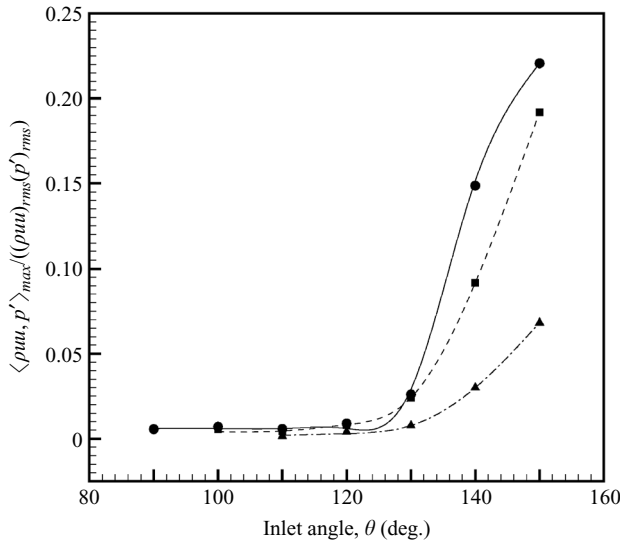
FIGURE 25. Directivity of normalized $\langle \rho uu, p' \rangle_{max}$ correlation. Laser probe locations are at $r/D = 0$, $x/D = 12$ (Mach 1.8), 10 (Mach 1.4 and Mach 0.95). $\bullet$, $M = 1.8$; $\blacksquare$, $M = 1.4$; $\blacktriangle$, $M = 0.95$.

All direct correlation data presented in this paper are from two different single-stream jet facilities at the NASA Glenn Research Center. The first one is an unheated facility used for high-subsonic and supersonic jets. The second one is a heated jet facility. This facility was used to measure the bulk of the jet-flow turbulence far-field correlation data presented in this paper. In both facilities, the primary air stream was filtered to remove dust particles. In addition, a low-speed ($\sim$15 m s$^{-1}$) clean co-flowing stream was created around the primary jet to block entrainment of the dust-laden ambient air. A hydrogen combustor was used in the heated facility to avoid soot particles.

In the correlation experiments, the far-field sound pressure fluctuations were measured using microphones mounted on a $50D$ (diameter) arc for the unheated jet and $100D$ for the heated jet facility. The laser probe volume (for Rayleigh-scattering measurements) was traversed on an $(x, r)$-plane ($x$: axial, $r$: radial directions) containing the jet centreline, while the microphone was kept fixed. The microphone and the Rayleigh-scattering data were acquired simultaneously. The synchronization was thoroughly checked using independent means.

For all the data presented below, the positive maximum of the correlation function is used. In the work of Panda *et al.* (2002, 2005), the data were normalized by the local root-mean-squared values of the measured variables. This, however, does not provide a comparison of the absolute levels of the correlation function. The absolute level of the correlation function is a measure of the noise source strength. In this investigation, we normalize some of the correlation data by a common reference value (denoted by subscript *ref*). In this way, the normalized data are used to identify dominant noise source location, relative strength and directivities.

### 4.1. *Direct correlation data*

The direct correlation data measured by Panda and coworkers are remarkable and quite unexpected. Figures 25 and 26 show directivity plots of the maximum of the measured normalized correlations. These figures are basically figures 12(*a*) and 12(*b*)
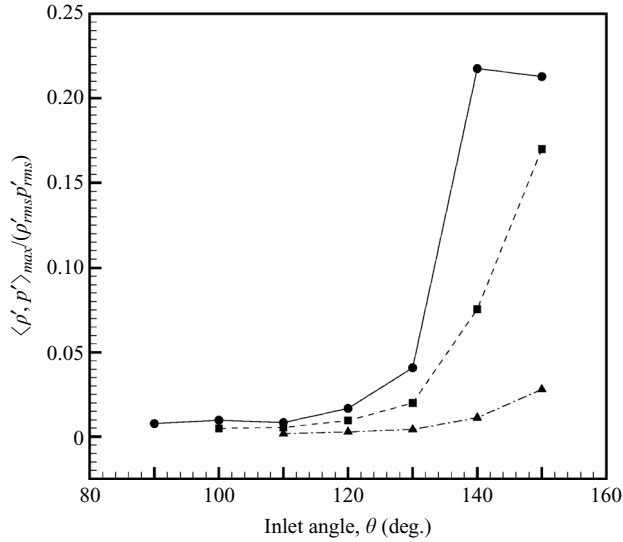
FIGURE 26. Directivity of normalized $\langle \rho', p' \rangle_{max}$ correlation. Laser probe locations and Mach numbers are the same as in figure 25.

of Panda *et al.* (2005); but there are some errors in their figures 12(*a*) and 12(*b*). The correct data are presented here in figures 25 and 26. In measuring these data, the laser probe was kept fixed at the centreline of the jet at $x/D = 12$ for the Mach 1.8 jet and $x/D = 10$ for the Mach 1.4 and Mach 0.95 jets. The far-field microphone was moved at $10°$ intervals on a circular arc. Figure 25 shows the directivity of the normalized $\rho uu$ correlation, that is $\langle \rho uu, p' \rangle_{max} / [(\rho uu)_{rms}(p')_{rms}]$. Figure 26 shows the directivity of $\langle \rho', p' \rangle_{max} / (\rho'_{rms} p'_{rms})$. Here, a prime represents the deviation from the mean. These directivity data are important. First, they reveal that there are significant correlations between jet turbulence fluctuations at a point inside the jet and the sound field radiated in the downstream direction. This is true regardless of which turbulence related fluctuation is used. Since the Rayleigh scattering measurements are concentrated in a very localized volume in the jet, a $20\%$ correlation is a huge number. Another significance of the data is that the normalized correlation drops off rapidly as the inlet-angle direction decreases. For angles less than $120°$, the correlation practically diminishes to the noise level. The directivity pattern as given by figures 25 and 26 does not change when the laser probe is moved radially over the half-width of the jet and axially over a few jet diameters. This indicates that the direct correlation function and noise sources are highly directional.

It is clear from figures 25 and 26 that the noise source measured by the laser probe exhibits strong directional characteristic. It radiates noise primarily in the downstream direction. There is practically no noise radiation to the sideline and upstream directions. Panda and his coworkers were fully aware of this unusual characteristic. They offered an explanation for the observed directional variation based on the two-noise source model. For the purpose of completeness, we will amplify their reasoning below, using the fine-scale turbulence and large turbulence structure noise source model of figure 4.

The two-noise source model of figure 4 suggests that the dominant source of noise radiating to the sideline and upstream directions is the fine-scale turbulence of the jet flow. In measuring the turbulence fluctuations in a jet by the Rayleigh-scattering
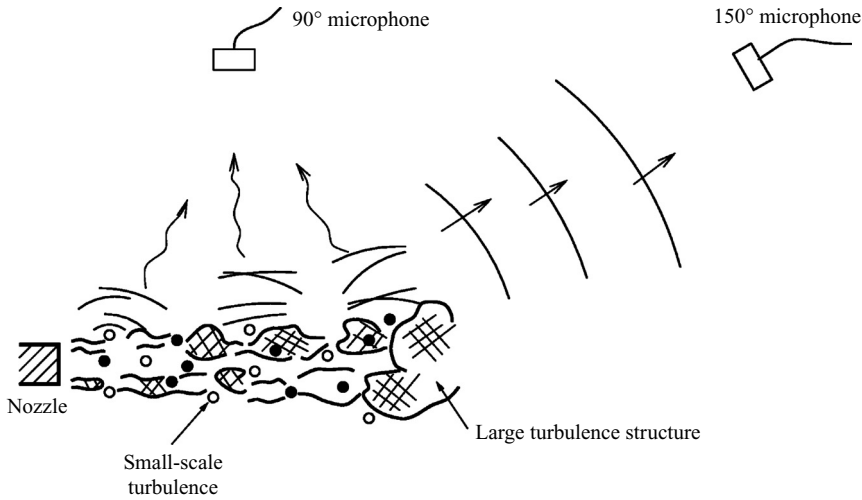
FIGURE 27. Schematic diagram of the sources of jet noise radiating to the side line and the downstream directions.

technique, the fluctuations measured are associated with small blobs of turbulence. The pressure signal, measured by a far-field microphone at, say, 90°, however, comes from the numerous blobs of turbulence of the entire jet (see figure 27). Thus, the intensity of the acoustic pressure from the blob of turbulence in the measurement volume of the laser probe is miniscule. It is totally overwhelmed by the noise from all the other blobs of small-scale turbulence in the jet. Thus, we should expect very low to no correlation between far-field pressure and laser probe signal.

The two-noise source model in figure 4 also suggests that the large turbulence structure noise is coherent and Mach wave-like. It is highly directional and radiates primarily in the downstream direction. Now the signal from the laser probe, although very localized, is, in fact, representative of that of the large turbulence structures. The large turbulence structures radiate a significant fraction of the sound measured by the far-field microphone, say, at 150° (see figure 27). Therefore, the turbulent motion that generates the signal at the laser probe is also responsible for a significant fraction of the noise received by the microphone. Thus, according to this model, there should be reasonable correlation between the laser probe and the microphone signals. This explains why the amplitude and shape of the direct correlation is as shown in figures 25 and 26. In a nutshell, the correlation data reflects the contributions from the large turbulence structures and their noise alone.

The experimental results of figures 25 and 26 are extremely important. They provide clear evidence of the existence of two very different noise sources and hence offer direct support to the two-noise source model elaborated in §1. Further, it confirms that the noise radiated to large inlet angles in the downstream direction is from the large turbulence structures of the jet flow. This provides the required experimental validation of associating the peaky similarity spectrum of figure 2 to the noise from the large turbulence structures throughout the previous two sections. In these two figures, the correlation drops rapidly around 140° to 130°. This implies that the large turbulence structure noise is confined to the cone $\theta \geqslant 130°$ for cold jets at high subsonic to moderately supersonic Mach numbers. This drop-off angle compares well with the dominance-change-over angle evident in figures 6 (OASPL data), figures 7 (peak Strouhal number data), figures 9 and 10 (power law data) of single far-field
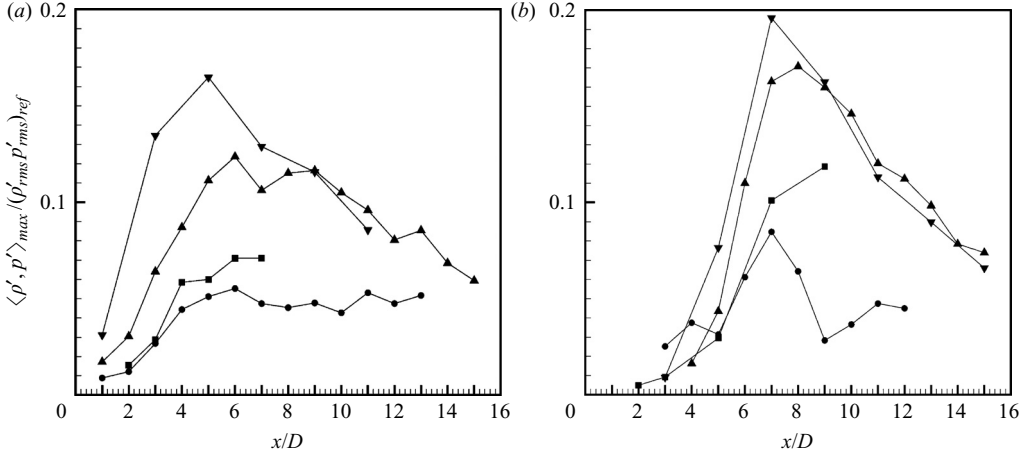
FIGURE 28. Measured spatial distributions of $\langle \rho', p' \rangle_{max}/(\rho'_{rms}, p'_{rms})_{ref}$ for Mach 0.9 jets. (a) $x/D$ is the location of the laser probe along the nozzle lip line $r/D = 0.5$. (b) $x/D$ is the location of the laser probe along the jet centreline $r/D = 0$. The far-field microphone is at $150°$. ●, $T_r/T_a = 1.0$; ■, 1.43; ▲, 1.82; ▼, 2.7.

microphone data in §2 and figures 14 and 15 (autocorrelation data) as well as figures 21 and 22 (two-microphone correlation data) of §3. Taken collectively, we believe all these different types of experimental results not only are consistent with each other but also provide coherent and firm support for the two-noise source model of figure 4.

## 4.2. *Noise source location and intensity*

Based on the above observations, it appears that it is possible to use direct correlation data to provide an idea of the noise source location and intensity associated with the large turbulence structures. To do so, it is necessary to process the correlation data so that they are normalized with respect to a common reference. Such normalized data allow a comparison of the intensities of correlations at different radiation directions and laser probe locations. In turn, the data provide a measure of the relative noise source intensity. We would like to point out that the $\rho'_{rms}$ at a fixed location in the jet and $p'_{rms}$ at a fixed direction in the far-field arc as measured, did experience minor variations from day to day. These minor variations, however, appear to be random. They have not been removed from the data as they have little impact on the conclusions to be drawn.

Figure 28(a) shows the normalized density–pressure correlation curves for four Mach 0.9 jets. In measuring the correlation data, the laser probe is moved axially along the nozzle lip line at $r/D = 0.5$. The far-field microphone is fixed at $150°$. The reference $\rho'_{rms}$ is the value at $r/D = 0$, $x/D = 7.0$ and the reference $p'_{rms}$ is the value measured when the microphone was placed at $150°(T_r/T_a = 1.0)$. Measurements were made at jet temperature ratio $T_r/T_a = 1.0$, 1.43, 1.82 and 2.70. Jet noise experiments have shown that at a fixed Mach number, the noise from a jet increases with jet temperature ratio. Thus, in the present experiment, the highest temperature jet emits most noise. In other words, the noise source strength of the $T_r/T_a = 2.70$ jet is strongest. Figure 28(a) shows that the normalized correlation data $\langle \rho', p' \rangle_{max}/(\rho'_{rms}, p'_{rms})_{ref}$ do increase with jet temperature. This confirms the expectation that $\langle \rho', p' \rangle_{max}/(\rho'_{rms}, p'_{rms})_{ref}$ (direct correlation normalized by a common reference root-mean-squared value) is, indeed,
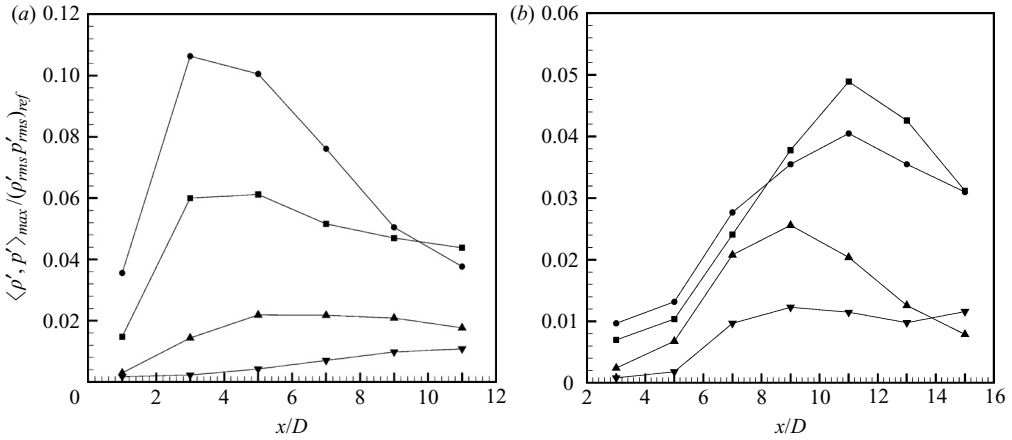
FIGURE 29. Spatial distributions of $\langle \rho', p' \rangle_{max}/(\rho'_{rms}, p'_{rms})_{ref}$ for a Mach 1.48 jet at $T_r/T_a = 2.27$, (a) $r/D = 0.5$, (b) $r/D = 0$. ●, $\theta = 150°$; ■, 140°; ▲, 130°; ▼, 120°.

a measure of the noise source strength. Figure 28(b) shows a similar plot along the centreline of the jet. Again, the higher the temperature ratio (the stronger is the noise radiated) the larger is the normalized direct correlation. The results of figures 28 provide a validation of the proposition that $\langle \rho', p' \rangle_{max}$ is a measure of the noise source strength.

Figure 29(a) shows the axial distribution of $\langle \rho', p' \rangle_{max}/(\rho'_{rms}, p'_{rms})_{ref}$ for a supersonic jet at Mach 1.48 and jet temperature ratio 2.27. Here, $(\rho'_{rms})_{ref}$ is the value at $r/D = 0.5$, $x/D = 3.0$ and $(p'_{rms})_{ref}$ is the value at inlet angle 150°. The data was measured along the nozzle lip line at $r/D = 0.5$. The nozzle lip line is almost the centreline of the shear layer surrounding the jet. The four curves in this figure give the relative noise source distributions radiating to $\theta = 150°$, 140°, 130° and 120°, respectively. This figure indicates that there is a large increase in noise source strength as the (inlet angle) direction of radiation increases. The noise source strength drops rapidly to an insignificant value for radiation angle less than 120°. In other words, for a supersonic jet, the large turbulence structure noise is highly directional and confined to the downstream direction. All these features are consistent with far-field noise data presented in §2. In addition, this figure reveals that the peak noise source in the jet shear layer moves upstream with an increase in the direction of radiation. This is new and has not been reported before. Figure 29(b) shows similar relative noise source strength distributions along the centreline of the jet. In contrast to that along the jet shear layer, the noise source strength peaks at a location slightly downstream of the end of the potential core and moves further downstream with increase in angle of radiation. On comparing figures 29(a) and 29(b), it appears that, for moderately supersonic jets, sources in the jet shear layer produce somewhat more noise than sources along the jet centreline.

Figure 30 is similar to figure 29 but for a subsonic jet at Mach 0.6 and temperature ratio 2.27. The $(\rho'_{rms})_{ref}$ value in this figure is that measured at $r/D = 0$ and $x/D = 7.0$. The $(p'_{rms})_{ref}$ value is that measured at inlet angle 150°. At this subsonic jet Mach number, the noise source strength of the large turbulence structures is low compared to the Mach 1.48 supersonic jet in figure 29. In addition, the dominant noise source is now located slightly downstream of the end of the potential core around the jet centreline. Further, significant noise source strength is found only for radiation to
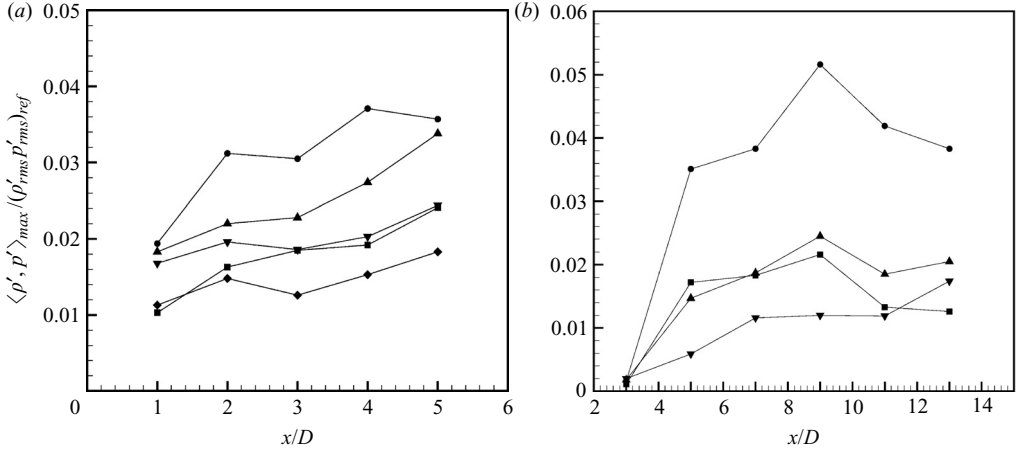
FIGURE 30. Spatial distributions of $\langle \rho', p' \rangle_{max}/(\rho'_{rms}, p'_{rms})_{ref}$ for a Mach 0.6 jet at $T_r/T_a = 2.27$, (a) $r/D = 0.5$, (b) $r/D = 0$. ●, $\theta = 150°$; ▲, $140°$; ■, $130°$; ▼, $120°$; ◆, $110°$.

very large inlet angle (150°). A detailed explanation of this observation is beyond the scope of this work. However, it is reasonable not to expect Mach wave radiation from a subsonic jet except at the end of the potential core of the jet where there is a rapid decay of the large turbulence structures. The rapid decay process creates supersonic wave components (see §1), which lead to Mach wave radiation.

## 5. Jet noise source distribution via acoustic mirror measurements

To complement the noise source location results of the direct correlation data of the previous section, jet noise source distribution measurements have been carried out using an elliptic mirror microphone. Acoustic mirror microphones have previously been used in Schlinker (1975), Chu & Kaplan (1976), and Laufer et al. (1976). The elliptic mirror microphone experiments of this investigation were conducted at the Boeing Low Speed Aeroacoustics Facility. Detailed description of the test facility, data acquisition and reduction process may be found in Viswanathan (2003) and will not be repeated here. The aperture of the Boeing elliptic mirror is 1.5 m (4.92 ft) and the length of the semi-major axis is 2 m (6.73 ft). As noted in the previous section, direct correlation data provide the noise source directivity and location of the large turbulence structures only. The data offer no information on the noise sources associated with fine-scale turbulence. One important advantage of using an elliptic mirror microphone is that it measures the noise from both large turbulence structures and fine-scale turbulence of the jet flow. Thus, the elliptic mirror microphone is a valuable tool for jet noise source study.

### 5.1. Elliptic mirror microphone

To provide a better understanding of the measured data, it is useful to examine the principle of the elliptic mirror microphone. Figure 31 shows a schematic diagram of an elliptic mirror microphone. The inside surface of the instrument is a part of an ellipsoid of revolution. It has two foci. The measurement microphone is housed at the near focus and the source of interest at the far focus. For applications to jet noise, the far focus is typically located on the jet centreline. Consider the acoustic ray L1 and the reflected ray L2. The combined path length (L1 + L2) controls the relative phase between the acoustic rays arriving at the microphone via different parts of the mirror.
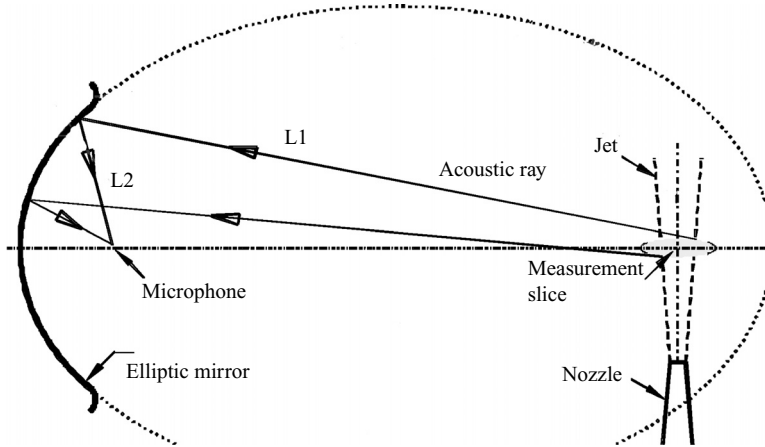
FIGURE 31. Schematic diagram of an elliptic mirror microphone for jet noise source measurements.

When the source is at the far focus, the combined distance (L1 + L2) is constant and the microphone senses a strong signal; but if the source is displaced transversely from the major axis of the mirror, the path lengths begin to vary and there is destructive interference, resulting in a drop in the strength of the sensed signal. Thus, the mirror has the desirable property of distinguishing between sources that are located on the far focus from those that are displaced in the transverse or lateral directions. It should be kept in mind though that the resolution is not a sharp point, but a small region near the far focus.

When the source is located on the major axis of the mirror but not at the focus, the response of the mirror is different. The response is insensitive since the variations in the path lengths from different reflection paths from the mirror are much less than for transverse offset of the source. That is, the mirror does not distinguish between sources that are located along the major axis of the mirror, within a certain range. Therefore, it does not differentiate between sources located on the near (front) and far (back) shear layers of the jet (see figure 31). This lack of sensitivity in the direction of the mirror major axis is a useful property, in that it allows the mirror to 'listen' to an entire slice of the jet. The measurements should, therefore, be interpreted as the total noise radiated by the axial slice of the jet. The spatial resolution is a strong function of the source frequency. Higher frequencies are better resolved since the same difference in path lengths results in a larger phase difference. The reduced resolution of the lower-frequency waves is a problem associated with all microphone array techniques.

### 5.2. *Noise source distributions*

The intent of the present noise source distribution measurements is to show there is a difference between that of the fine-scale turbulence and those of the large turbulence structures. Since noise sources are distributed along the length of a jet, a simple way to observe changes in noise source distribution is to focus on the location of the peak level. For convenience, the noise source distribution for a given direction of radiation is presented as the variation of OASPL (in dB) per unit length of jet with distance downstream, $x/D$, from the nozzle exit. Thus for this type of plot, the area under the curve is the OASPL for that direction. Since all the measured distributions have a single dominant peak, the higher the peak level, the stronger the noise radiation in that direction. Figure 32 shows the measured axial distribution of the relative OASPL
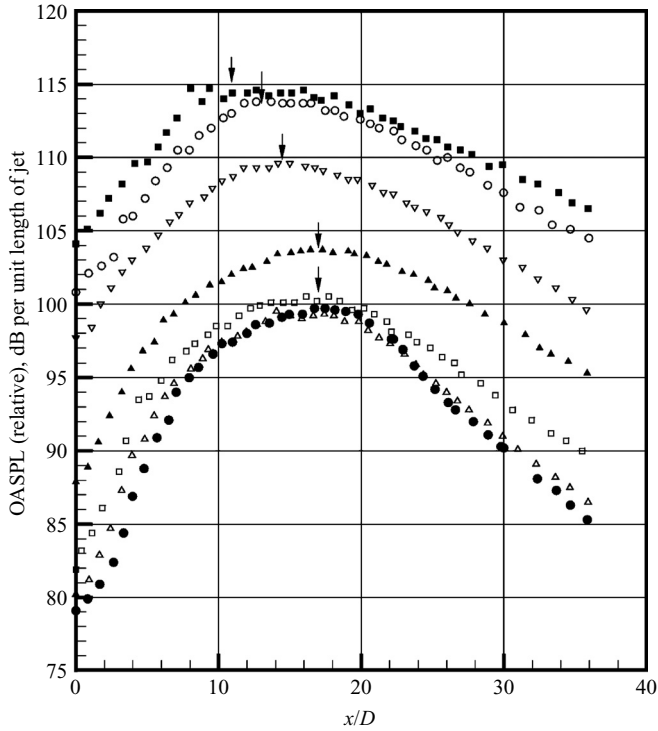
FIGURE 32. Measured axial distributions of relative noise source strength of a Mach 1.9 jet at temperature ratio 1.0. ●, $\theta = 90°$; △, $100°$; □, $110°$; ▲, $120°$; ▽, $130°$; ○, $140°$; ■, $150°$. Arrow indicates location of maximum level.

of the noise source strength per unit length of a Mach 1.9 jet at temperature ratio 1.0 for various directions of radiation. At this high Mach number, most of the noise is radiated in the downstream direction. As a result, the OASPL source level is much higher in the downstream direction. There is a rapid drop in the level of noise source strength between $140°$ and $110°$ (figure 32). Based on the observations and conclusions of the previous sections, it is reasonable to regard the noise source distributions for $90°$, $100°$ and $110°$ radiation as that of the fine-scale turbulence. Also, it is reasonable to regard the noise source distributions for radiating to $130°$, $140°$ and $150°$ as those of the large turbulence structures. One obvious observation is that the $90°$ to $110°$ noise source distributions all peak at the same location (in figure 32 and subsequent figures, the location of the peak level of noise source distribution is indicated by a small arrow), slightly downstream of the end of the potential core. This suggests that the noise source or the fluctuations in kinetic energy of the fine-scale turbulence is at its highest level there. As discussed before, the direction of radiation of small blobs of turbulence is statistically isotropic. It is, therefore, not surprising that the noise source distribution is insensitive to the direction of radiation (the slight shift in noise level is due mainly to the source convection effect mentioned before). On the other hand, the noise source distribution curves for radiation from $130°$ to $150°$, as shown in figure 32, do not peak at the same location. The peak location moves upstream with increase in the (inlet) angle of radiation. This is consistent with direct correlation measurements of large turbulence structure noise source for a supersonic jet (see figure 29a). At the present time, we do not know the reason behind this phenomenon. Figure 33 shows
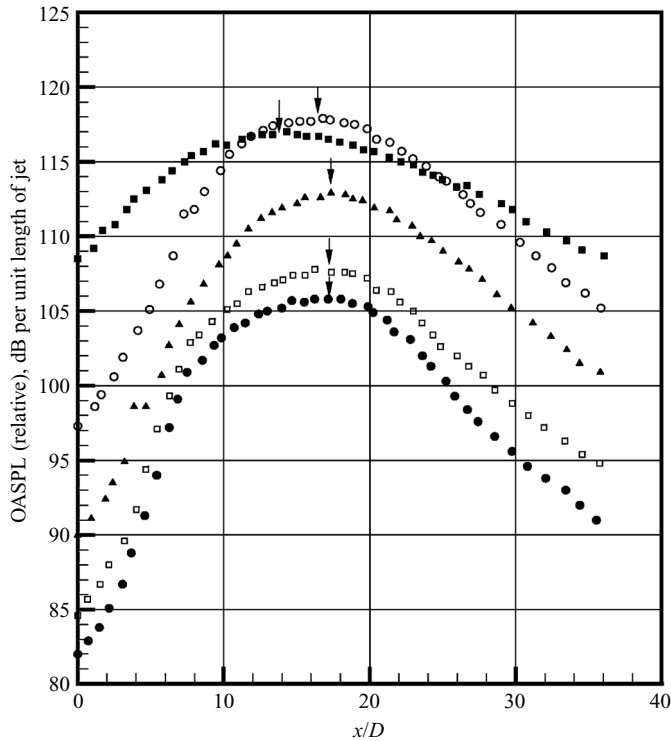
FIGURE 33. Measured axial distributions of relative noise source strength of a Mach 1.9 jet at temperature ratio 2.2. ●, $\theta = 90°$; □, $100°$; ▲, $110°$; ○, $120°$; ■, $150°$. Arrow indicates location of maximum level.

the measured noise source distributions again for a Mach 1.9 jet but at a temperature ratio 2.2. It exhibits similar characteristics as the temperature ratio 1.0 jet.

The above observation that the fine-scale turbulence noise sources of a supersonic jet are concentrated in a region slightly downstream of the end of the potential core is also true for subsonic jets. This can readily be seen in figures 34 and 35 for a Mach 0.9 and a Mach 0.5 jet. In these figures, the noise source distribution curves for radiation to the sideline all peak at about the same location. Similarly, the observation that the locations of the peaks of noise source distributions of large turbulence structures (radiating to large inlet angles) change with direction of radiation is also true for subsonic jets. This characteristic behaviour of jet noise source distribution is evidence that reinforces our belief that there are two types of noise source in high-speed jets.

## 6. Conclusion

In this investigation, four types of experimental data are measured and analysed in an effort to establish what are the sources of jet noise. They include single microphone far-field noise data, two-microphone far-field correlation data, correlations of jet turbulence fluctuations, measured by the Rayleigh-scattering technique, and far-field microphone signal, and noise source distribution data from acoustic mirror measurements. It is our opinion that all the data sets that have been analysed, both independently and collectively, point to one single conclusion; that there are two
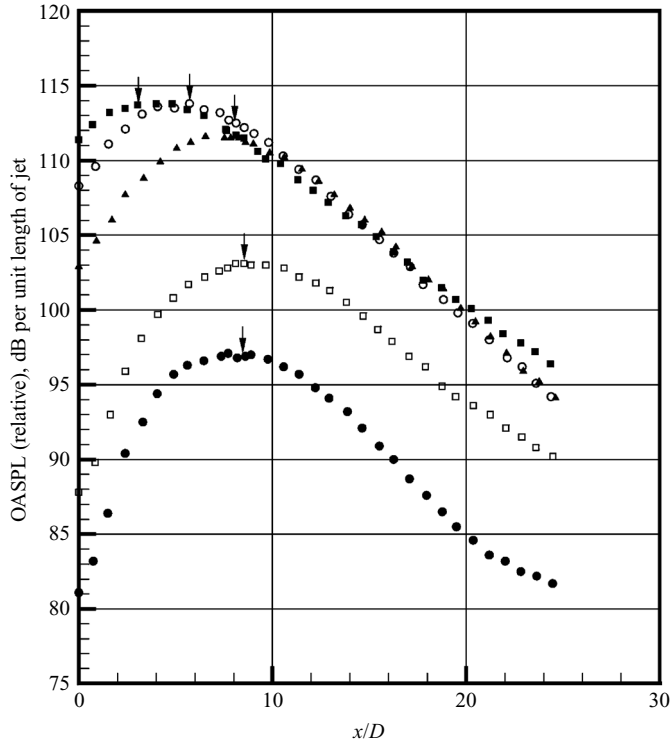
FIGURE 34. Measured axial distributions of relative noise source strength of a Mach 0.9 jet at temperature ratio 3.2. ●, $\theta = 90°$; □, 110°; ▲, 130°; ○, 140°; ■, 150°. Arrow indicates location of maximum level.

distinct sources of jet noise. They are the fine-scale turbulence and the large turbulence structures of the jet flow.

The single- and two-microphone far-field data, provide insight and information concerning the acoustic field. The data show clearly that the noise field is made up of two components, each with distinct characteristics. The sound field in the downstream sector is coherent radially and along any polar arc. This is consistent with the proposition that it is generated by the coherent large turbulence structures of the jet flow. The sound field in the sideline directions is random with large-frequency bandwidth and little spatial correlation. This is consistent with the proposition that it is generated by the fine-scale turbulence of the jet flow. Direct correlations between turbulent fluctuations measured inside the jet and far-field pressure signal reveal that there is significant correlation if the microphone is placed at a large inlet angle direction. For sideline and upstream directions, there is little to no correlation. This result is consistent with the recognition that only the contributions from the large turbulence structures are measured by this method. The directivity of the direct correlation function is similar to the directivity of large turbulence structures noise. Hileman and coworkers (Hileman *et al.* 2003, 2004, 2005) used simultaneous acoustic measurements and real-time flow visualization in jets to determine the sources of noise. Their technique was designed to observe only the noise from large turbulence structures. Their results are similar and complementary to the present direct correlation data. An acoustic mirror measures the axial noise source strength distribution in a jet. The instrument measures the noise from fine-scale turbulence as
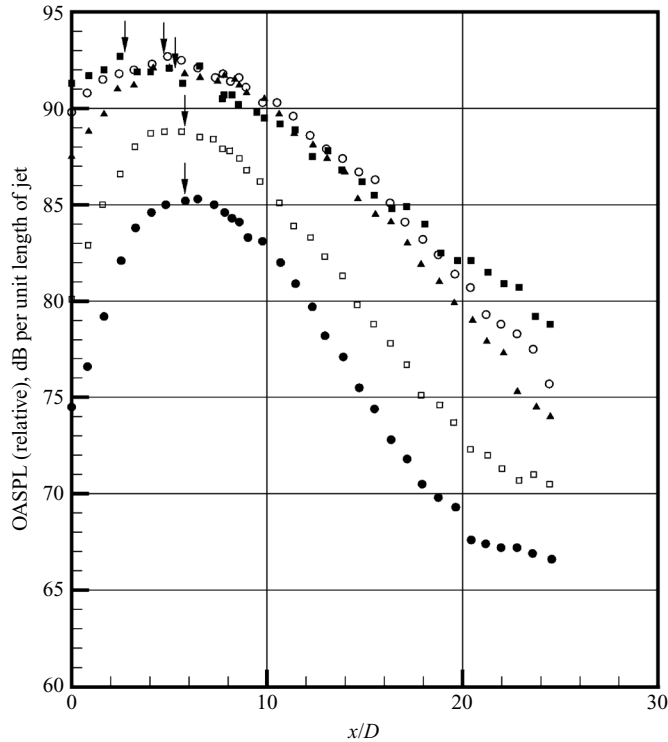
FIGURE 35. Measured axial distributions of relative noise source strength of a Mach 0.5 jet at temperature ratio 3.2. ●, $\theta = 90°$; □, 110°; ▲, 130°; ○, 140°; ■, 150°. Arrow indicates location of maximum level.

well as from large turbulence structures. It is observed in the present investigation that the dominant part of fine-scale turbulence noise source is located just downstream of the potential core of the jet. This is true regardless of the direction of radiation. On the other hand, the location of the peak noise source strength for radiation in the downstream direction (dominated by the noise of large turbulence structures) moves upstream with an increase in the (inlet) angle of radiation. This result is consistent with that of direct correlation.

What are the sources of jet noise? This has been a long-standing controversy. Theoretical approaches following the Lighthill acoustic analogy, invariably, draw the conclusion that the sources are quadrupoles. With advances in computational aeroacoustics methods and the availability of fast computers, it becomes feasible to simulate numerically the turbulent jet flows and the associated noise radiation. However, because a computation domain must be finite and relatively small, methods other than direct computation have to be used to extend the numerical solution to the far-field. Most investigators choose to use the acoustic analogy method or a variant of it. For simplicity, we will refer to all these methods as acoustic analogy. As a result, this has led many computational investigators to suggest that quadrupoles rather than turbulence are the sources of jet noise. One notable exception is the work of Bogey & Bailly (2005). Bogey & Bailly also used the acoustic analogy to extend their computed solution to the far-field; but instead of simply attributing the noise sources to quadrupoles, they processed their numerical data to unravel the noise sources. Their conclusion supports the two-noise source model.

Based on the experimental evidence presented in this paper, we are convinced that the physical sources of jet noise are the fine-scale turbulence and the large turbulence structures of the jet flow. Mathematically, it is well known that we can use equivalent sources to predict a given noise field. Equivalent sources are mathematical sources that are not necessarily real or physical. This is possible because of the famous theorem on the 'inverse problem'. That is, given a radiation field, we cannot uniquely determine its sources. This 'inverse problem', however, does not apply to the present work for we measure the direct correlation between the source fluctuations and the sound field. Knowing the physical sources is definitely very important. For noise-suppression purposes, we must find out what the physical sources are. Thus far, it appears that jet noise suppression methods or devices have been developed largely on a trial and error basis. It is hoped that future efforts in jet noise suppression will focus on suppressing the large turbulence structures as they are the dominant sources of jet noise.

## REFERENCES

ATVARS, J., SCHUBERT, L. H. & RIBNER, H. S. 1965 Refraction of sound from a point source placed in an air jet. *J. Acoust. Soc. Am.* **37**, 168–170.

BOGEY, C. & BAILLY, C. 2005 Investigation of sound sources in subsonic jets using causality methods on LES data. *AIAA Paper* 2005–2885.

BROWN, G. L. & ROSHKO, A. 1974 On density effects and large structures in turbulent mixing layers. *J. Fluid Mech.* **64**, 775–816.

CHU, W. T. & KAPLAN, R. E. 1976 Use of a spherical concave reflector for jet noise source distribution diagnostics. *J. Acoust. Soc. Am.* **59**, 1268–1277.

CROW, S. C. & CHAMPAGNE, F. H. 1971 Orderly structures in jet turbulence. *J. Fluid Mech.* **48**, 547–591.

DAHL, M. D. & PAPAMOSCHOU, D. 2000 Analytical predictions and measurements of the noise radiated from supersonic coaxial jets. *AIAA J.* **38**, 584–591.

DOAK, P. E. 1960 Acoustic radiation from a turbulent fluid containing foreign bodies. *Pro. R. Soc. Lond.* A **254**, 129–145.

FFOWCS-WILLIAMS, J. E. 1963 The noise from turbulence convected at high speed. *Trans. R. Soc. Lond.* A **255**, 469–503.

GOLDSTEIN, M. E. 2003 A Generalized acoustic analogy. *J. Fluid Mech.* **488**, 315–333.

GOLDSTEIN, M. E. & ROSENBAUM, B. M. 1973 Effect of anisotropic turbulence on aerodynamic noise. *J. Acoust. Soc. Am.* **54**, 630–645.

HILEMAN, J., THUROW, B. & SAMIMY, M. 2003 Exploring noise sources using simultaneous acoustic measurements and real-time flow visualization in jets. *AIAA J.* **40**, 2382–2392.

HILEMAN, J., THUROW, B. & SAMIMY, M. 2004 Development and evaluation of a 3-D microphone array to locate individual acoustic sources in a high-speed jet. *J. Sound Vib.* **276**, 649–669.

HILEMAN, J. CARABALLO, E., THUROW, B. & SAMIMY, M. 2005 Large-scale structure evolution and sound emission in high-speed jets: real-time visualization with simultaneous acoustic measurements. *J. Fluid Mech.* **544**, 277–307.

HUNTER, C. & THOMAS, R. H. 2003 Development of a jet noise prediction method for installed jet configuration *AIAA Paper* 2003–3169.

HURDLE, P. M., MEECHAM, W. C. & HODDER, B. K. 1974 Investigation of the aerodynamic noise generating region of a jet engine by means of the simple source fluid dilatation model. *J. Acoust. Soc. Am.* **56**, 1708–1721.

KHAVARAN, A. KREJSA, E. A. & KIM, C. M. 1994 Computation of supersonic jet mixing noise from an axisymmetric convergent-divergent nozzle. *J. Aircraft* **31**, 603–609.

KOPIEV, V. F., CHERNYSHEV, S. A., ZAITSEV, M. Y. & KUZNETSAV, V. M. 2006 Experimental validation of instability wave theory for round supersonic jet. *AIAA Paper* 2006–2595.

LAUFER, J., SCHLINKER, R. H. & KAPLAN, R. E. 1976 Experiments on supersonic jet noise. *AIAA J.* **14**, 489–497.

LEE, H. K. & RIBNER, H. S. 1972 Direct correlation of noise and flow of a jet. *J. Acoust. Soc. Am.* **52**, 1280–1290.

LIGHTHILL, M. J. 1952 On sound generated aerodynamically: I. General theory. *Proc. R. Soc. Lond.* A **211**, 564–581.

LIGHTHILL, M. J. 1954 On sound generated aerodynamically: II. Turbulence as a source of sound. *Proc. R. Soc. Lond.* A **222**, 1–32.

LILLEY, G. M. 1958 On the Noise from air jets. *Aeronaut. Res. Council Rep. Mem.* **20**, 376.

MAESTRELLO, L. 1976 Two-point correlation of sound pressure in the far-field of a jet. *NASA TM* X–72835.

MORRIS, P. J. & FARASSAT, F. 2002 Acoustic analogy and alternative theories of jet noise. *AIAA J.* **40**, 671–680.

NORUM, T. D. & BROWN, M. C. 1993 Simulated high speed flight effects on supersonic jet noise. *AIAA Paper* 93–4388.

PANDA, J. 2007 Experimental investigation of turbulence density fluctuations and noise generation from heated jets. *J. Fluid Mech.* **591**, 73–96. (See also *AIAA Paper* 2004-3016.)

PANDA, J. & SEASHOLTZ, R. G. 2002 Experimental investigation of density fluctuations in high-speed jets and correlation with generated noise. *J. Fluid Mech.* **450**, 97–130.

PANDA, J., SEASHOLTZ, R. G. & ELAM, K. A. 2005 Investigation of noise sources in high-speed jets via correlation measurements. *J. Fluid Mech.* **537**, 349–385.

PHILIPS, O. M. 1960 On the generation of sound by supersonic turbulent shear layer. *J. Fluid Mech.* **9**, 1–28.

PROUDMAN, I. 1952 The generation of noise by isotropic turbulence. *Pro. R. Soc. Lond.* A **214**, 119–132.

RIBNER, H. S.1964 The generation of sound by turbulent jets. In *Advances in Applied Mechanics*, vol. 8, pp. 108–182. Academic.

RICHARZ, W. G. 1980 Direct correlation of noise and flow of a jet using laser Doppler. *AIAA J.* **18**, 759–765.

SCHAFFAR, M. 1979 Direct measurements of the correlation between axial in-jet velocity fluctuations and far-field noise near the axis of a cold jet. *J. Sound Vib.* **64**, 73–83.

SCHLINKER, R. H. 1975 Supersonic jet noise experiments. PhD thesis, Department of Aerospace Engineering, University of Southern California.

SEASHOLTZ, R. G., PANDA, J. & ELAM, K. A. 2001 Rayleigh scattering diagnostics for dynamic measurement of velocity fluctuations in high speed jets. *AIAA Paper* 2001–0847.

SEASHOLTZ, R. G., PANDA, J. & ELAM, K. A. 2002 Rayleigh scattering diagnostics for measurement of velocity and density fluctuation spectra. *AIAA Paper* 2002–0827.

SEINER, J. M., PONTON, M. K. JANSEN, B. J. & LAGEN, N. T. 1992 The effects of temperature on supersonic jet noise emission. *AIAA Paper* 92–2046.

SIDDON, T. E. 1973 Noise source diagnostics using causality correlations. *AGARD CP* 131, 7-1–7-13.

TAM, C. K.W. 1995 Supersonic jet noise. *Annu. Rev. Fluid Mech.* **27**, 17–43.

TAM, C. K. W. 1998 Influence of nozzle geometry on the noise of high speed jets. *AIAA J.* **36**, 1396–1400.

TAM, C. K. W. 2006 Dimensional analysis of jet noise data. *AIAA J.* **44**, 512–522.

TAM, C. K. W. & AURIAULT, L. 1999 Jet mixing noise from fine-scale turbulence. *AIAA J.* **37**, 145–153.

TAM, C. K. W. & BURTON, D. E. 1984*a* Sound generated by instability waves of supersonic flows. Part 1. Two-dimensional mixing layers. *J. Fluid Mech.* **138**, 249–272.

TAM, C. K. W. & BURTON, D. E. 1984*b* Sound generated by instability waves of supersonic flows. Part 2. Axisymmetric jets. *J. Fluid Mech.* **138**, 273–295.

TAM, C. K. W. & CHEN, K. C. 1979 A statistical model of turbulence in two-dimensional mixing layers. *J. Fluid Mech.* **92**, 303–326.

TAM, C. K. W. & CHEN, P. 1994 Turbulent mixing noise from supersonic jets. *AIAA J.* **32**, 1774–1780.

TAM, C. K. W. & ZAMAN, K. B. M. Q. 2000 Subsonic jet noise from non-axisymmetric and tabbed nozzles. *AIAA J.* **38**, 592–599.

TAM, C. K. W., GOLEBIOWSKI, M. & SEINER, J. M. 1996 Two components of turbulent mixing noise from supersonic jets. *AIAA Paper* 96–1716.

TESTER, B. J. & MORFEY, C. L. 1976 Development in jet noise modelling–Theoretical predictions and comparisons with measured data. *J. Sound Vib.* **46**, 79–103.

THUROW, B. SAMIMY, M. & LEMPERT, W. 2003 Compressibility effects on turbulence structures of axisymmetric mixing layers. *Phys. Fluids* **15**, 1755–1765.

VAN DYKE, M. 1982 *An album of Fluid Motion,* Parabolic Press, Stanford, California.

VISWANATHAN, K. 2002 Analysis of the two similarity components of turbulent mixing noise. *AIAA J.* **40**, 1735–1744.

VISWANATHAN, K. 2003 Jet aeroacoustic testing: issues and implications. *AIAA J.* **41**, 1674–1689.

VISWANATHAN, K. 2004 Aeroacoustics of hot jets. *J. Fluid Mech..* **516**, 39–82.

VISWANATHAN, K. 2006 Scaling laws and a method for identifying components of jet noise. *AIAA J.* **44**, 2274–2285.

VISWANATHAN, K. 2007 Investigation of the sources of jet noise. *AIAA Paper* 2007–3601.

YAMAMOTO, K., BRAUSCH, J. F., JANARDAN, B. A., HOERST, D. J., PRICE, A. O. & KNOTT, P. R. 1984 Experimental investigation of shock-cell noise reduction for single-stream nozzles in simulated flight, *Test Nozzle and Acoustic Data, Comprehensive Data Report*, vol. 1, NASA CR–168234.